Texas A&M University
Mechanical Engineering Department
Turbomachinery Laboratory

Dynamic Forced Response of a Rotor-Hybrid Gas Bearing System due to Intermittent Shocks

Research Progress Report to the Turbomachinery Research Consortium

TRC-B&C-1-08

by

Keun Ryu
Research Assistant

Luis San Andrés
Mast-Childs Professor
Principal Investigator

May 2008

Dynamic Forced Response of a Rotor-Hybrid Gas Bearing System due to Intermittent Shocks

Executive Summary

Gas bearings in Micro-turbomachinery (MTM) offer significant system level benefits, such as improved fuel efficiency reductions in weight and number of components, extending life cycle and maintenance intervals, and reducing NOX emissions with a lower CO_2 footprint. Emerging opportunities of gas bearings range from automotive turbochargers to engines for business jet aircraft, for example. Gas bearings, because of the inherently low gas viscosity, have low damping relative to oil-lubricated bearings and are prone to wear during rotor start-up and shut down procedures. The lack of damping brings concerns about rotor-gas bearing system robustness and endurance to tolerate shock induced loads, sudden while landing in jet engines or intermittent while moving across rough terrain in vehicles, for example.

In 2008, sporadic shock loads are exerted to the base of an existing rotor-gas bearing system while coasting down from a top speed of 60 krpm (1000 Hz). In the tests, (1) an electromagnetic pusher delivers impacts to the rig base, or (2) the whole rig is manually tilted and dropped. The test rig consists of a rigid rotor, 0.825 kg and 28.6 mm in diameter, supported on two hybrid, flexure pivot tilting pad type, gas bearings, each with four pads and 60% pivot offset and 0.6 mm feeding holes. The bearings are supplied with feed pressure of 2.36, 3.72, and 5.08 bar (ab). Intermittent shocks, up to 30 g pk-pk and broad frequency range to 400 Hz, produce a remarkable momentary increase of the overall rotor response amplitude, up to 50 μm (pk-pk). The shocks readily excite the natural frequency of the rotor-bearing system (150-200 Hz), and on occasion the natural frequency (40 Hz) of the whole test rig. For operation at rotor speeds above the system critical speed, the rotor synchronous response is isolated; with transient motions induced by a shock, subsynchronous in whirl frequency, quickly disappearing. Full recovery takes place in ~0.10 second. The measurements demonstrate that the hybrid gas bearings have enough damping to rapidly attenuate rotor transient motions and to dissipate the energy induced from intermittent shocks. Note that shocks acted while the rotor traversed its critical speeds! The reliability of the gas bearings to forced transient events is no longer in question.

TABLE OF CONTENTS

LIST OF TABLES

LIST OF FIGURES

NOMENCLATURE

A	Amplitude of acceleration [m/s^2]
A_p	Peak amplitude of acceleration [m/s^2]
C_b	Radial bearing clearance [m]
C_p	Radial pad clearance [m]
d_o	Feed orifice diameter [m]
D_b	Bearing diameter [m]
I_p	Pad mass moment of Inertia [kg-m^2]
K_{eff}	Effective stiffness coefficient [N/m]
$K_{\delta\delta}$	Web rotational stiffness [Nm/rad]
L	Bearing axial length [mm]
m	Fraction of the rotor mass that each bearing supports [kg]
R_p	Pad radius [m]
R_j	Rotor radius [m]
t	Time [s]
ξ	Damping ratio
τ	Shock time duration [s]
ω_c	Critical speed [rad/s]

Acronyms

LH, LV	Left bearing, horizontal and vertical planes
MTM	Micro-turbomachinery
N.F.	Natural frequency
RH, RV	Right bearing, horizontal and vertical planes

Introduction

Microturbomachinery (MTM) implements gas bearings to increase mechanical efficiency and to improve reliability, while reducing overall system weight, and operating at high rotational speeds and extreme temperature conditions. Proven gas bearings with large damping and load capability, preferably of simple configuration as well as low cost, will enable more successful commercial applications, such as turbochargers, auxiliary power units (APU) for aircrafts, and micro gas turbines (<400kW) [1]. Moreover, gas bearings satisfy environmental restrictions by eliminating contamination due to oil lubricating. Gases as a lubricant, are more stable (for example, no lubricant vaporization or cavitation, material solidification or decomposition) at extreme temperature and high rotor speeds. In general, however, gas bearings have little damping to attenuate rotor motion due to sudden imbalances and shock loads. In addition, gas bearings introduce excessive power losses and wear quickly during frequent rotor start and stop cycles. The thrust of the current work is to investigate reliable conventional and inexpensive gas bearings, easy to install and align, and constructed from common materials and processes.

Gas foil bearings (GFBs) are customarily used in commercial MTM because of their advantages over rolling element bearings including no *DN* limit, higher temperature operation, low maintenance and tolerance to debris and rotor misalignment [2]. However, the cost and lack of reliable predictive tools have limited the universal application of foil bearings in MTM.

The research at TAMU advances the technology of hybrid gas bearings for application into oil-free high performance MTM by demonstrating experimentally the bearings' rotordynamic performance, reliability, and durability [3]. The present work focuses on recording the dynamic forced performance of a rotor-gas bearing system operating under intermittent external shock conditions.

Shock tolerance of gas bearings is required to make them suitable for automotive and general aviation transportation applications. Turbochargers on diesel truck engines, for example, are customarily subjected to shocks transmitted from road surface conditions. The shocks can induce severe damage due to direct impact collisions or transient rubbing contact between the rotor and its bearings or other components. Prior to commercial usage, the operating performance and reliability of the rotor-gas bearing systems must be determined under externally imposed shock and vibration transmitted through the system foundation.

The present work demonstrates the robustness of hybrid gas bearings under severe operating conditions; i.e., shocks up to ~30 g (pk-pk) delivered to the test rig base. The test rotor-bearing system is subjected to intermittent multiple shocks suddenly induced by large external impacts.

The transient response of a small rigid rotor, 0.825 kg and 28.6 mm in diameter, supported on two flexure pivot tilting pad hybrid gas bearings is measured using two different excitation methods:

(a) applying impacts to the rig support base via an electromagnetic pusher, and

(b) by manually tilting the test rig base to various heights and dropping it.

Rotor speed deceleration tests are conducted to characterize the rotor response. The test bearings are supplied with increasing feed pressures during both normal operation (i.e., no shock) and shock loads tests.

Literature review on rotor-bearing systems subjected to external shocks

MTM typically operates at high temperatures and rotational speeds to achieve desired power and efficiency and to reduce pollutants. Elimination of oil-lubricated bearings and associated lubrication system provides dramatic system level benefits, i.e., weight reduction, fuel efficiency improvements, maintenance and logistic support reductions, and decreased life cycle costs [1, 4]. Gas bearings are most attractive for high performance MTM. For example, oil-free TCs eliminate oil coking and seal failure problems while providing mounting and installation freedom [5]. References [6~9] include extensive literature reviews on the state of art in gas bearings for oil-free MTM.

However, gas bearings have a relatively lower load capacity, direct stiffness and damping coefficients, than oil-lubricated bearings because the viscosity of the gas is inherently small [10]. The static and dynamic forced performance characteristics of gas bearings can be enhanced by reducing the bearing clearances or by increasing the operating speed [11]. However, fabrication processes for bearings with minute clearance increase overall manufacturing and installation costs. Furthermore, minute bearing clearances can lead to severe transient rotor-bearing contact and rubbing when the system is subject to sudden shock loads.

Spencer et al [12] conduct comprehensive shock impact tests on a rotor-gas bearing system simulating a Bryton cycle turbocompressor (10~15 kW). Two tilting pad (four pads)

gas bearings and a spiral-grooved thrust bearing support the test rotor, 4.76 kg in weight and 38.1mm in diameter. The test bearing surfaces are coated with plasma-sprayed chrome oxide (operating temperature up to ~300°C). The bearings, with each pad supported on a flexure of radial stiffness equal to 0.35 MN/m, can accommodate rotor centrifugal growth and thermal expansion. Applied typical shock loads are half-sine pulses of ~40 g (pk-pk) with 10 ms time duration. Shocks are imposed to the test rig along the rotor horizontal, vertical and axial directions. While operating the test rig at a rotor speed of 39 krpm, the test rig is lifted pneumatically (drop height of ~ 2.5 cm) and then released to fall into an elastomer pad resting on a large base. The test gas bearings survive externally imposed 40 g shock loads, 10 ms in duration. Momentary contacts between the rotor and bearing surface are observed during the tests. The ability of the gas bearings to survive intermittent contact during high rotating speed condition relies strongly on the bearing coating materials.

Tessarik et al [13] investigate the effects of random vibrations on the dynamic response of a rotor-gas bearing system. Two tilting pad (three pads type) gas bearings and a step-sector thrust bearing support a turbine-driven rotor weighing ~9.5 kg, and with nominal operating speed of 36 krpm. Only one of the pivots in each bearing assembly is mounted on a flexure web (radial stiffness of 0.35 MN/m) and other pads are individually supported by the pivots. Random vibrations are applied by means of a large shaker at input levels ranging 0.5~1.5 g (rms). Since the base excitations are random, statistical analysis methods is used. The input random excitations have a normal or Gaussian distribution. The measured rotor responses are analyzed for amplitude distribution and power spectral density. Frequent contact of the rotor to the bearing surfaces occurs above 5.4 g (rms) shock loads. An experimental probability analysis shows that the dynamic response of the gas bearing supported rotor tends to shift toward non-Gaussian distributions as the external vibration input level increases because of the increasingly nonlinear stiffness coefficients of the gas film at decreasing film thicknesses.

Heshmat et al [4] and Walton et al [14] present shock tolerance tests on a rotor-gas foil bearing system. A test rotor, simulating a turbocharger (150 HP unit) and a miniature turbojet engine (290 N thrust), is operated up to 150 krpm rotor speed and with bearing temperatures of max. ~400°C. At selected rotor speeds ranging from 60 to 100 krpm, the test rig is elevated by a roll maneuver to a specified height and dropped. From the drop events, shock loads of 20~40 g (pk-pk) are applied to the whole test rig. The rotor transient responses quickly decay to a full recovery within 75 ms. The estimated log decrement from the rotor transient responses renders 0.3~0.4 (damping ratio of 4.8~6.4 %). Note that GFBs can accommodate

misalignment and unexpected excursions of the journal due to shock or sudden maneuvers because of the resilience of the gas foil bearing [15].

The literature on the dynamic response of rotors supported on rolling element bearings or oil-lubricated bearings to externally induced vibrations is quite extensive. Analyses focus on general movements of bases, particularly for seismic excitation, see Refs. [16-18]. Subbiah et al [19] investigate the effects of support stiffness and damping on the transient rotor response due to base random excitations. The amplitude power spectral densities due to random support excitations for rotor response are calculated using modal analysis method. A flexible rotor, with single disk at the center of the shaft supported on two oil-lubricated bearings, is modeled. Significant amplitude rotor responses along the vertical direction can occur due to the excitation along the rotor horizontal direction and vice-versa because of the bearing cross-coupled force coefficients.

Lee et al. [20] investigate experimentally the transient response of a flexible rotor to base-transferred shock excitation. Electromagnetic shaker-induced shock experiments are performed with a series of half-sine shock waves, up to 3 g, of duration time of 5~15 ms. The test rotor is supported on two ball bearings. The transient response of the rotor is sensitive to the duration time of the shocks. When the frequencies of the shock waves are close to the critical speed of the rotor-bearing system, resonances occur and the transient response of the rotor is amplified. In Ref. [21], the same authors propose a generalized FE analysis model to predict the transient response of a flexible rotor-bearing system with mount systems to base-transferred shock forces. Duchemin et al [22] also conduct experiments for a flexible rotor, with a rigid disk, subjected to base excitation (sinusoidal accelerations). The test rotor, supported on two ball bearings, has a length of 0.4 m and a diameter of 10 mm. One end of the test rig base is linked to an electromagnetic shaker via a connecting push rod. Because of the rigid support bearings, the maximum acceleration applied to the rig for safe operation of the rotor-bearing system is 0.75 g.

The few publications referred to above [4, 12-14] present the dynamic response of rotors supported on gas bearings under sudden shock loads. To assess the effects of external shocks on gas bearing robustness, acquiring reliable test data on the rotordynamic performance of a gas bearing supported rotor under shock loads become essential.

Experimental Facility

Figure 1 depicts the layout of the gas bearing test rig and its instrumentation for rotordynamic measurements and application of impact loads. San Andrés and Ryu [9, 23] fully describe the components of the test rig and the supply air system into the test bearings. The apparatus consists of a rigid rotor supported on a pair of flexure pivot tilting pad hybrid bearings housed in a steel main body integrating a brushless AC motor armature (three-phase bi-polar configuration). The AC motor maximum speed is 99 krpm[1]. Three alignment bolts, 120° apart, position the test bearings within their housings. Piezoelectric load cells are installed between the bearing housing and each alignment bolt to measure the dynamic forces transmitted to the rig casing. Two pairs of eddy current sensors, orthogonally positioned and facing the rotor ends, measure vibration amplitudes of the test rotor along the vertical and horizontal planes. An infrared tachometer mounted at the right end of the rotor is a keyphasor signal for data acquisition.

The test rotor, 0.825 kg in mass, has a length of 190 mm and an outer diameter of 28.25 mm at the bearing location. The test flexure pivot hydrostatic gas bearings, made of bronze, have four arcuate 72° pads and 60% pivot offset. Figure 2 and Table 1 present the main dimensions of the test bearings. Each pad is connected to the bearing casing through a thin structural web with a (designed) rotational stiffness ($K_{\delta\delta}$) of 20 Nm/rad. From previous extensive experiments reported in Refs. [9, 23, 24], the test bearings' pads are worn, with each pad having an uneven clearance along the circumference and axial directions. Appendix A details the present pads' radial clearances on the test bearings.

[1] For the test bearings, maximum *DN* value with the equipped motor, where $D{\cdot}N$ = (diameter in mm) × (rotating speed in rpm), is ~ 2.9×10^6.

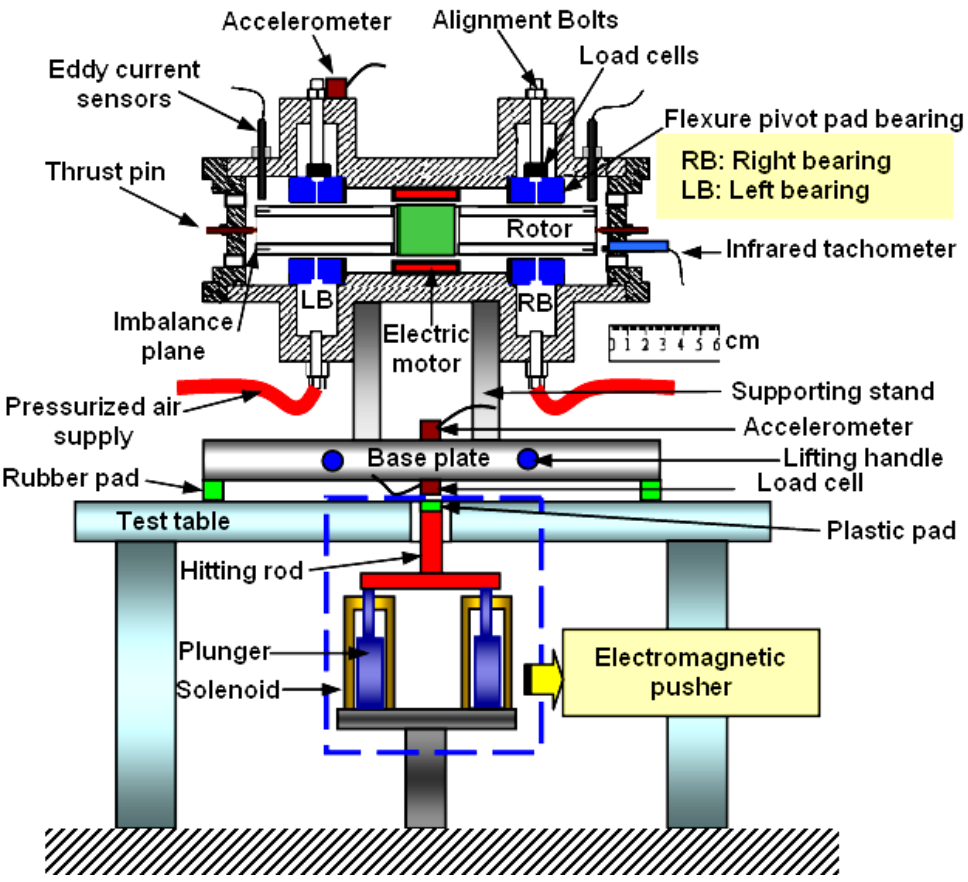

Fig. 1 Layout of gas bearing test rig and instrumentation

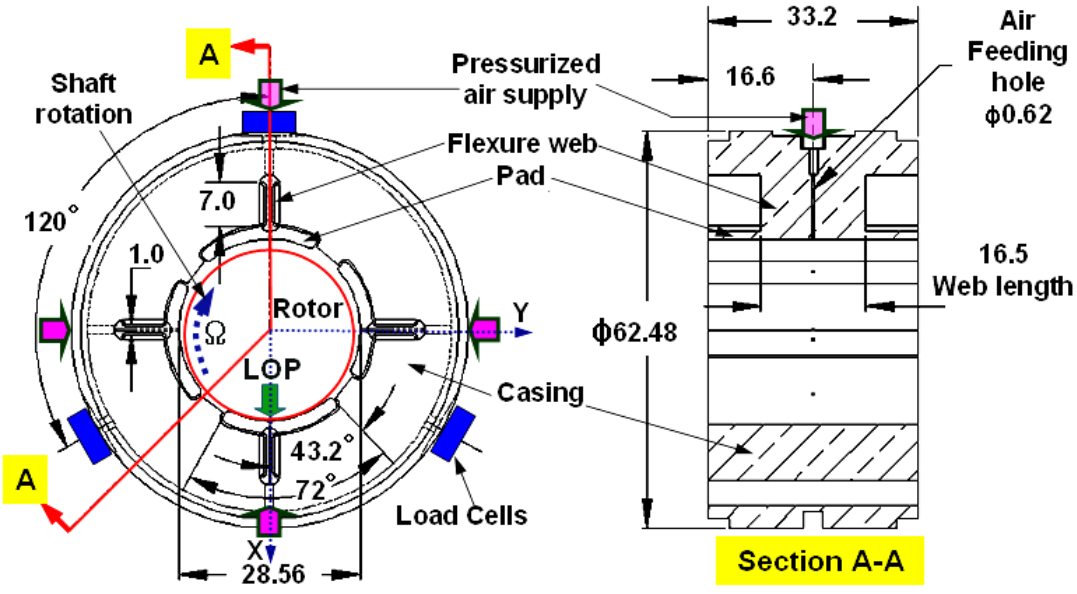

Fig. 2 Dimensions of test flexure pivot pad hybrid gas bearing (units: mm)

Table 1. Geometry of test flexure pivot bearings*

Parameter	Magnitude	Unit
Bearing axial length, L	33.2	mm
Pads number and arc length	4 (72 °)	
Pad pivot offset	60%	
Nominal preload	0.2	
Pad mass moment of inertia, I_p	0.253	g-mm^2
Web rotational stiffness, $K_{\delta\delta}$	20	Nm/rad
Number of feed orifices	4	
Feed orifice diameter, d_o	0.62	mm

(* Bearing material: Bronze)

The base plate supporting the test rig, see Figs. 1, 3, 4, can be manually rotated around a hinged fixture. Four rubber pads are attached to the bottom of the base plate to level the test rig and to isolate its vibration from the support table. Two lifting handles are secured at one end of the base plate to raise the test rig to various heights. Note that the whole test rig weighs ~48 kg. Appendix B details measured natural frequencies at various locations on the test rig for excitations delivered with a soft impact hammer (excitation frequency < 300 Hz). A distinct natural frequency of ~40 Hz, lightly damped, is recorded at the bearing housings and test rig base plate.

An in-house built fixture, named as an electromagnetic pusher (e-pusher), is installed under the support table, to deliver shock loads to the base of the test rig. The e-pusher consists of two identical push type solenoids; each, composed of a coil with an associated iron circuit forming the fixed part. The solenoid requires 37 watt at 10.5 volt input power and provides up to 240 N (54 lbf) at 2.54 mm (1 inch) stroke[2]. A moving iron plunger is pulled into the coil when the solenoid is energized. Removing power allows the plunger to return to its original position. A momentary push switch operates the solenoids. The hitting rod, which connects the plungers of both solenoids, as shown in Figs. 1 and 3, transmits the e-pusher loads through a piezoelectric load cell, affixed with a magnetic mount base to the bottom of the test rig base plate. This load cell, sensitivity of 0.22 mV/N and maximum compressive load of 44.5 kN, measures the applied shock load to the test rig. A *soft* plastic pad covers the tip of the hitting rod.

Two accelerometers are magnetically affixed to the test rig; one on the base plate, and the other atop the left bearing housing. These sensors measure the test rig dynamic acceleration

[2] The push force developed by the solenoid depends upon the number of coils of wire in the solenoid, its length, current through it, and the magnetic properties of the plunger [25].

at each location. Sensitivities of the accelerometers on the test rig base plate and left bearing housing are 9.99 mV/g and 5mV/g, respectively. The frequency ranges (±5%) for the sensors are 1~7k Hz and 1~10k Hz, respectively.

Commercial DAQ systems (*Bentley Nevada ADRE® for Windows* and *LabVIEW®*) collect and record the test data from coast down rotor speed experiments[3]. Table 2 shows the sampling size and acquisition rate of the *ADRE®* DAQ system. Note that the sampling size and rate of the *ADRE®* system depend on the rotor speed [26]. The sampling size and rate for *LabVIEW®* are 2018 (2^{11}) and 10,000 samples/sec[4], respectively. The DAQ systems records and stores new samples each time the rotor speed changes by 100 rpm and 1000 rpm for the *ADRE®* and *LabVIEW®* systems, respectively. A custom *LabVIEW®* graphical user interface (GUI) shows both time domain and frequency-domain representations of each signal during real time monitoring and data logging. A two-channel dynamic signal analyzer displays the frequency content of selected motion signals.

Table 2. Sampling size and rate of *ADRE* ® DAQ system

Rotor speed range [rpm]	Sampling size	Synchronous sampling rate [samples/revolution]
100 ~ 14,999	1024 (2^{10})	128 (2^{7})
15,000 ~ 29,999	512 (2^{9})	64 (2^{6})
30,000 ~ 60,000	256 (2^{8})	32 (2^{5})

Experimental Procedure

Rotor coast-down speeds tests from 60 krpm are conducted. In operation, the bearings are supplied with a supply pressure equal to 2.36, 3.72, and 5.08 bar (absolute). Only baseline rotor motions are measured (no added imbalance masses).

Two impulse load excitation methods are used to apply shock loads[5] to the test rotor-bearing system: (a) delivering impact loads to the test rig base plate utilizing the electromagnetic pusher (i.e., e-pusher test); and, (b) hand-lifting one end of the test rig base to various heights and dropping it (i.e., lift-drop test).

Figures 3 and 4 depict schematic views of the configuration for e-pusher tests and manual lift-drop tests, respectively. For each configuration, shock loads are transmitted to the test

[3] The maximum operating speed of *ADRE®* DAQ system is 60 krpm.
[4] Half the sampling frequency (i.e., Nyquist frequency) of DAQ system, 10 kHz/2=5 kHz, is the maximum FFT frequency avoiding aliasing.
[5] The mechanical shock is defined as a non-periodic (in the form of a pulse, a step, or transient vibration) vibratory excitation which is characterized by suddenness and severity [27].

bearings through the test rig base plate and bearing housing supports. Recall that two accelerometers are installed to measure the shock amplitude. One sensor (A1) rests on the test rig base plate, and the other one (A2) is atop the left bearing housing.

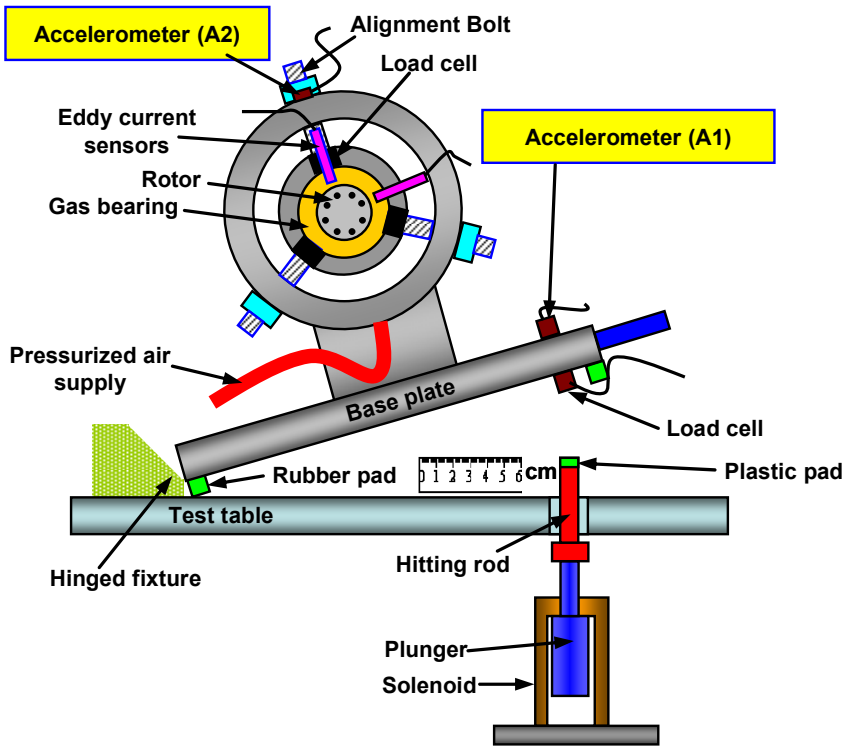

Fig. 3 Schematic view of electromagnetic pusher test

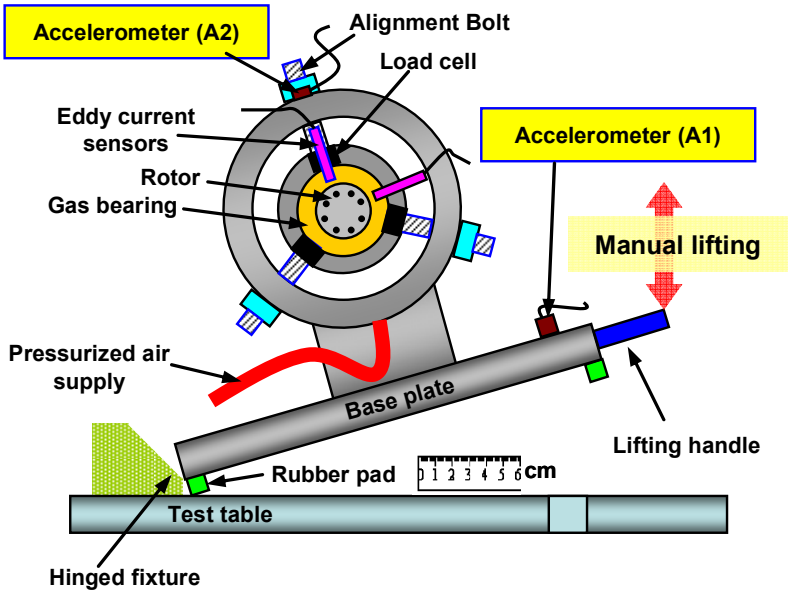

Fig. 4 Schematic view of manual lift-drop test

For e-pusher tests, shock loads are applied to the test rig while coasting down from a top speed (60 krpm) to rest. The impact forces render intermittent excitations to the whole test system. Figure 5 shows a typical measured impact force of the load cell under the test rig base place from a single impact delivered by the e-pusher. Note that the load cell serves as a trigger signal with a pre-trigger time of 0.2 second[6]. The typical impact duration is ~40 ms and the force delivered from the e-pusher is ~400 N (pk-pk). The excited frequency range does not exceed ~500 Hz. Recall that a *soft* plastic pad covers the tip of the hitting rod. Note that the impact duration and force amplitude are significantly dependent on the method of activating the solenoid, i.e., duration of switch activation. When the operator pushes and holds the momentary push switch longer, the impact time duration and load amplitude increases. Hence, the e-pusher offers intermittent impacts to the test rig.

Figure 6 depicts the measured shock loads from the accelerometer mounted on the test rig base plate under the impact e-force of Figure 5. The test rig is subjected to multiple impacts even with a single activation of the e-pusher because the test rig, after it is lifted by the e-pusher, drops until it hits the table.

The power to the motor controller is turned off to allow the rotor coasting down when the rotor speed reaches 60 krpm for manual base lift and drop tests. The test rig is then manually lifted off the test rig base plate to various heights (5~15 cm, 10~30° between the base plate and table) and dropped. Measured shocks record 10~30 g (pk-pk) depending on the drop height. Presently, four rubber pads are attached under the test rig base plate thereby affecting the drop shock amplitudes and excitation frequency range[7]. Figure 7 shows a typical recorded acceleration on the test rig base plate when the test rig is dropped once. The test rig experiences multiple shock loads since the test rig bounces after dropping.

[6] An infrared tachometer mounted at the rotor right end is a keyphasor signal for data acquisition during coast-down rotor speed tests.

[7] The highest peak impact forces excitation frequencies occur when there is a steel-on-steel (hard-on-hard) impact. The rubber supports reduce the shock load amplitude and excitation frequency range compared to when the test rig is dropped without rubber supports. In real operation of turbochargers for diesel or gasoline automotive engines, for example, the dynamic excitation of the vehicle from the road surface is transmitted through the vehicle's *soft* tires and suspension system.

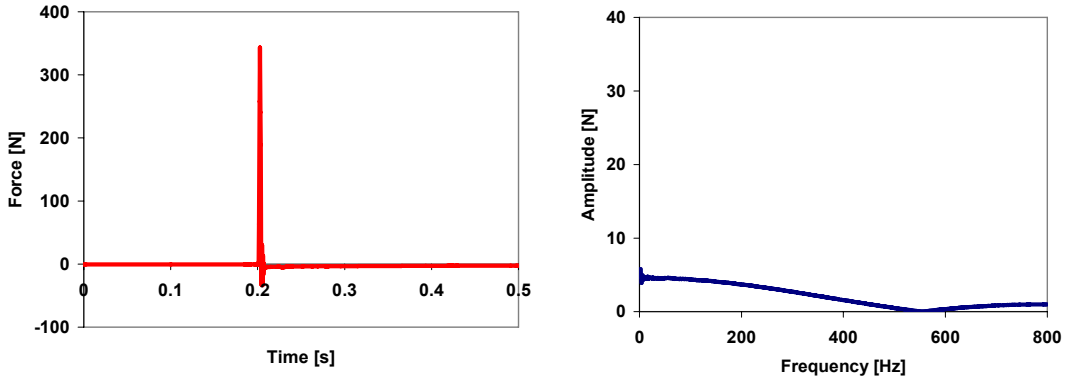

Fig. 5 Typical time signal and frequency spectrum of impact force from e-pusher. Pre-trigger 0.2 second.

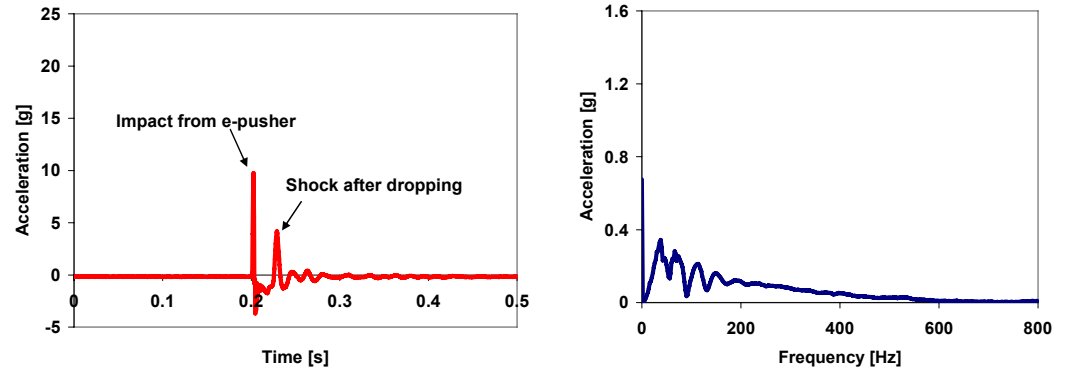

Fig. 6 Typical time signal and frequency spectrum of acceleration on test rig base plate under impact force (Fig. 5). Pre-trigger 0.2 second.

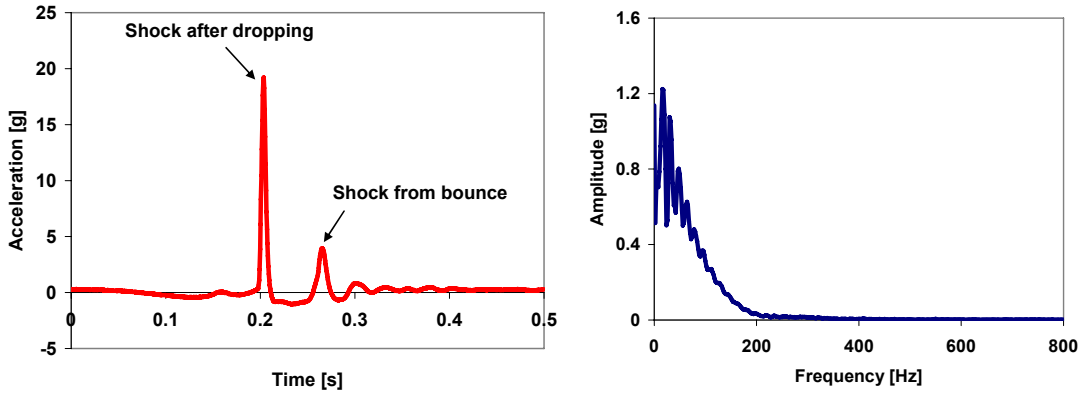

Fig. 7 Typical measured test rig base plate acceleration in time and frequency domains for lift-drop test. Pre-trigger 0.2 second.

Three parameters are necessary to describe a shock in the time domain: amplitude, duration, and shape [28]. Typical time duration and peak amplitude are 2.44 ms and 10.5 g for the e-pusher tests (Figure 6); and 13.67 ms and 19.5 g for the lift-drop tests (Figure 7), respectively. Figures 8 and 9 depict the measured shock pulse (zoomed from Figures 6 and 7) and two idealized shock pulses; half-sine and versed-sine[8] (haversine[9]) pulses obtained from the recorded time duration and a amplitude. The half-sine and versed-sine[10] pulses are calculated from $A(t)=A_p\times\sin(\pi t/\tau)$ and $A(t)=(A_p/2)\times(1-\cos(2\pi t/\tau))$, respectively [28], where A_p is the peak amplitude, t is time, and τ is time duration of the shock. The versed-sine best approximates the actual test shock pulse since shock loads are transmitted to the test rig through the rubber pads. Note that the versed-sine pulse represents typically an elastic impact [12]

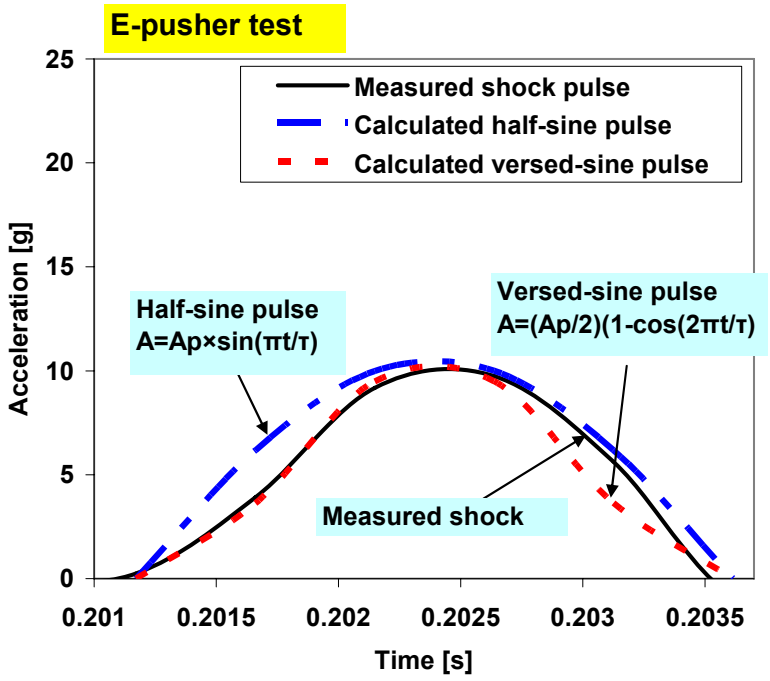

Fig. 8 Recorded shock pulse from e-pusher impact and calculated half-sine and versed-sine pulse. A_p: peak amplitude, t: time, τ: shock time duration.

[8] One minus Cosine
[9] One half of one minus Cosine
[10] The versed sine shape consists of an arc of sinusoid ranging between two successive minima [29].

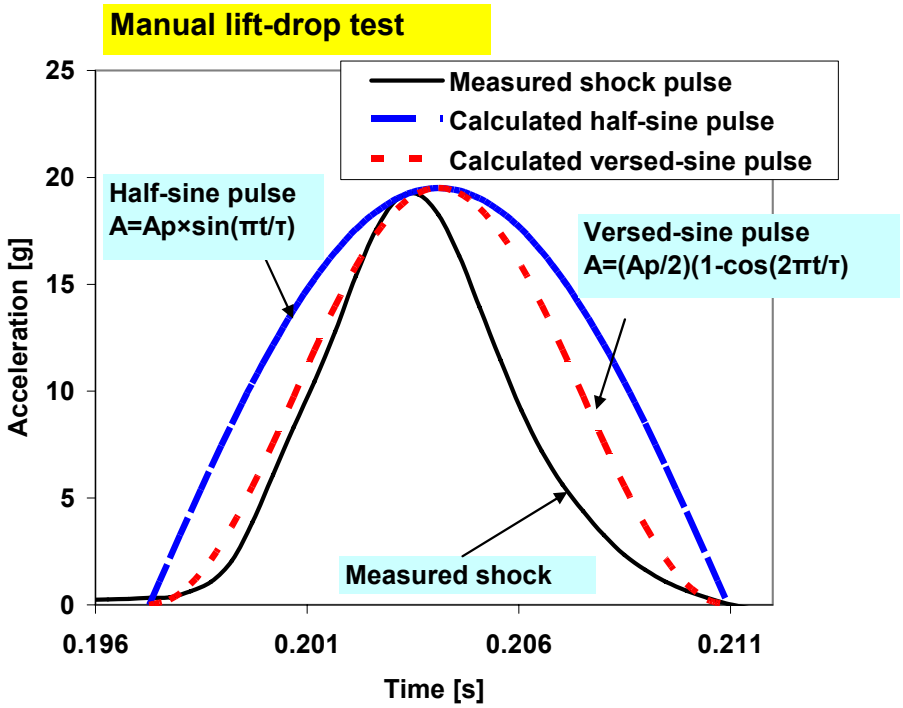

Fig. 9 Recorded shock pulse from drop impact and calculated half-sine and versed-sine pulse. A_p: peak amplitude, t: time, τ: shock time duration.

For the e-pusher tests and manual lift-drop tests, no shocks are imposed for rotor speeds below 10 krpm to avoid inaccurate slow roll compensation of the rotor response[11]. Slow roll compensation must be avoided when both the slow roll runout and the shock induced motion of the rotor cannot be easily discerned (separated).

Experimental Results

Baseline rotor response during normal operation (no shocks)

Figure 10 depicts the recorded amplitudes of synchronous rotor response for the test bearings feed with 5.08 bar (ab) pressure. This response is regarded as baseline. Slow roll compensation is conducted at 4 krpm[12]. Multiple peaks reveal the different forced response characteristics resulting from uneven clearances on each bearing pads; refer to Appendix A for details. Note that the overall clearance on the left bearing is much larger than that of the right bearing. The difference in force coefficients for the left and right bearings determines

[11] Slow roll compensation removes slow roll runout from a filtered vibration signal so that only the dynamic response of the rotor becomes dominant.
[12] The slow roll speed is typically less than 10% of the full operating speed of the rotor [30].

two rigid body conical modes, see Ref. [9]. Appendix C details the effect of supply pressure on the bearing dynamic force coefficients and lists the estimated rotordynamic parameters of the test rotor-bearing system extracted from measured synchronous speed rotor responses.

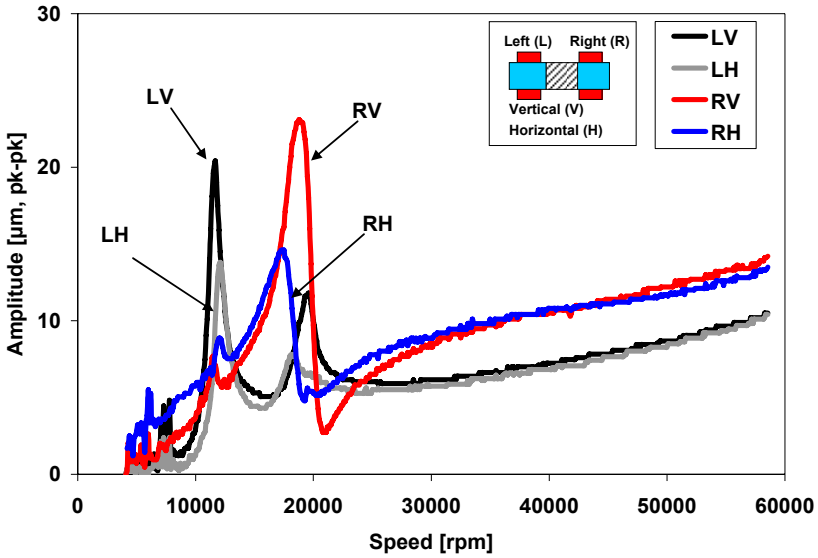

Fig. 10 Amplitude of rotor synchronous response versus rotor speed. 5.08 bar (ab) feed pressure into test bearings. Baseline condition.

For normal (no shock to the system) operation, Figures 11 and 12 depict waterfall plots and synchronous and subsynchronous vibrations of rotor coast down tests recorded at the horizontal direction of the rotor left end (LH) from a top speed (60 krpm) operating with 3.72 bar (ab) and 2.36 bar (ab) feed pressure, respectively. Recall that the system critical speeds along the LH direction for 3.72 bar and 2.36 bar feed pressures are 10.6 krpm (177 Hz) and 8.3 krpm (140 Hz), respectively.

For the bearings supplied with 3.72 bar pressure, see Figure 11, incipient subsynchronous vibration appears at rotor speeds above 52 krpm with a whirl frequency ratio (*WFR*) of ~ 0.2. The whirl frequency (215 Hz for 52~54 krpm, and 219 Hz for 55~58 krpm) is slightly higher than the system critical speed.

For bearings supplied with 2.36 bar feed pressure, as shown in Figure 12, large subsynchronous amplitudes are apparent at rotor speeds above 45 krpm and with a whirl frequency of 170~186 Hz[13]. The subsynchronous vibration amplitudes are twice or larger

[13] Small response amplitude, less than 10% of synchronous response amplitude, of 0.5X rotor vibration exists from 60 krpm to 45 krpm.

than the synchronous vibration amplitudes. Note that the subsynchronous frequencies increase from 170 to 186 Hz for rotor speeds between 45~58 krpm. The frequencies are a little higher than the natural frequency of the test rotor-bearing system, 8.3 krpm (140 Hz).

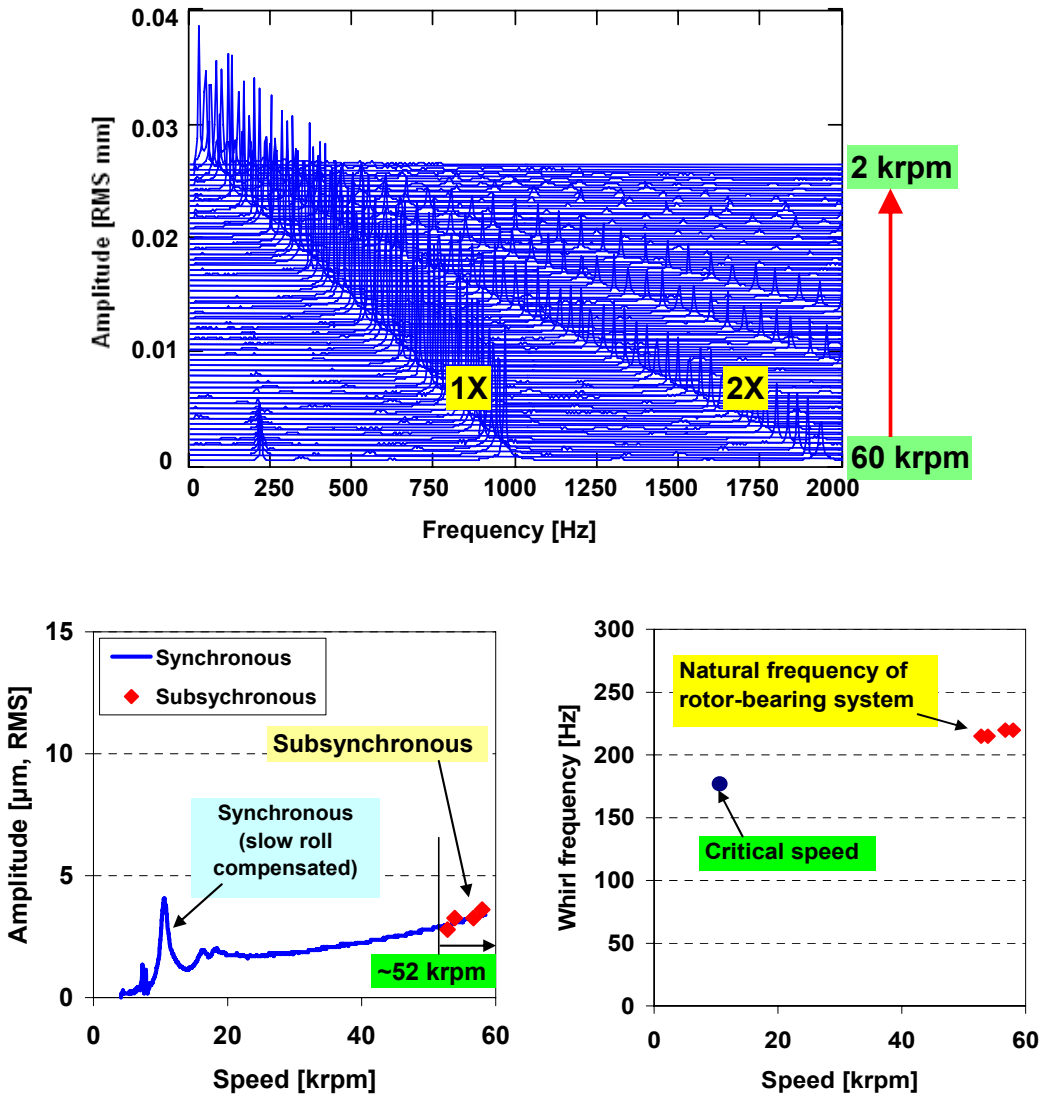

Fig. 11 Waterfall and amplitude of synchronous and subsynchronous rotor motions. 3.72 bar (ab) feed pressure. Measurements at rotor left end, horizontal plane (LH). Normal operation (w/o shocks).

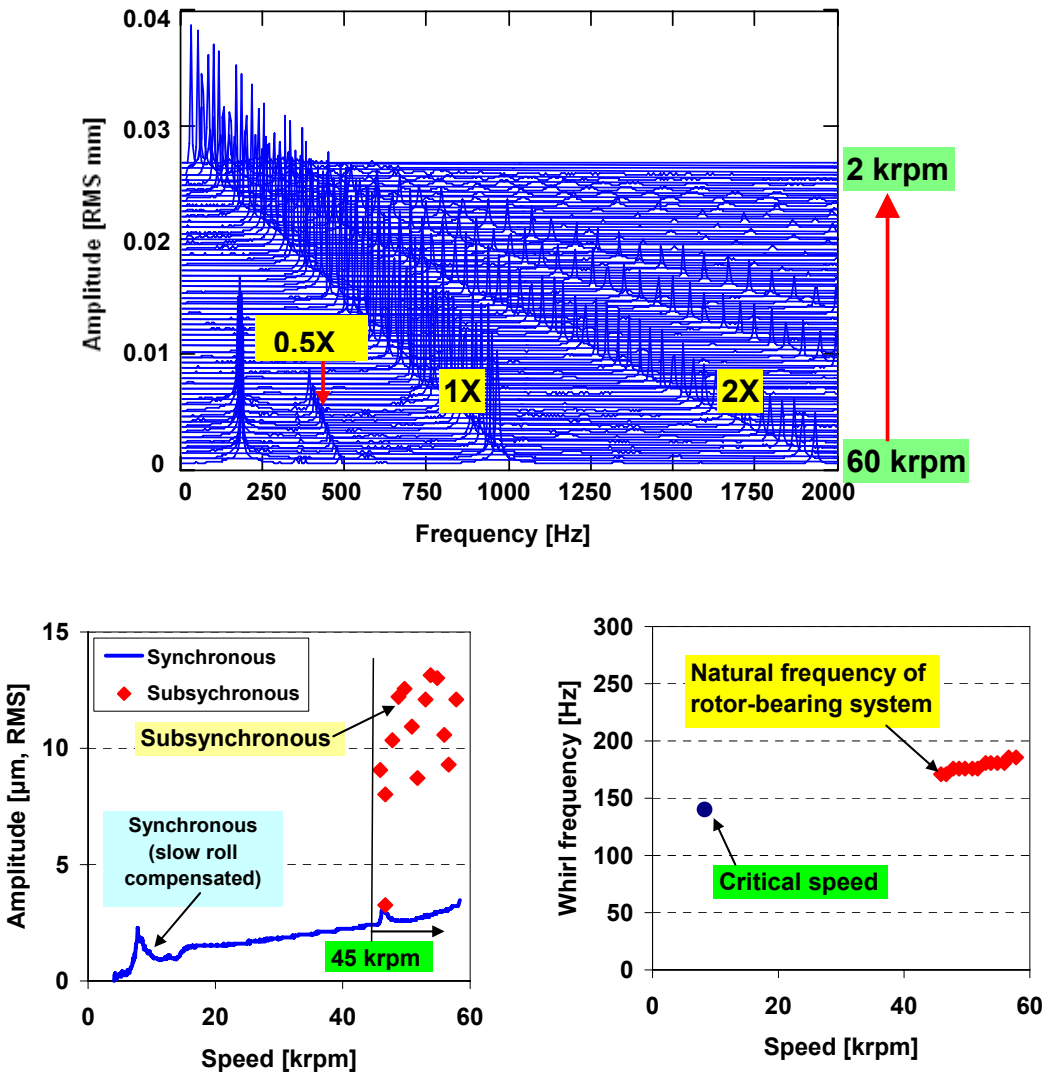

Fig. 12 Waterfall and amplitude of synchronous and subsynchronous rotor motions. 2.36 bar (ab) feed pressure. Measurements at rotor left end, horizontal plane (LH). Normal operation (w/o shocks).

Figure 13 depicts synchronous (1X) and 2X (frequency at twice of rotating speed) rotor response amplitudes for bearings supplied with 2.36 bar (ab) pressure. The 2X rotor response amplitude is almost constant at rotor speeds beyond the system critical speed though smaller than the synchronous rotor response amplitude, i.e., 60~70% of 1X amplitude below 20 krpm and ~45 % of 1X amplitude at 60 krpm. Recall that the drive AC motor has two poles. The magnetic forces in the motor render 2X rotor vibrations [31, 32].

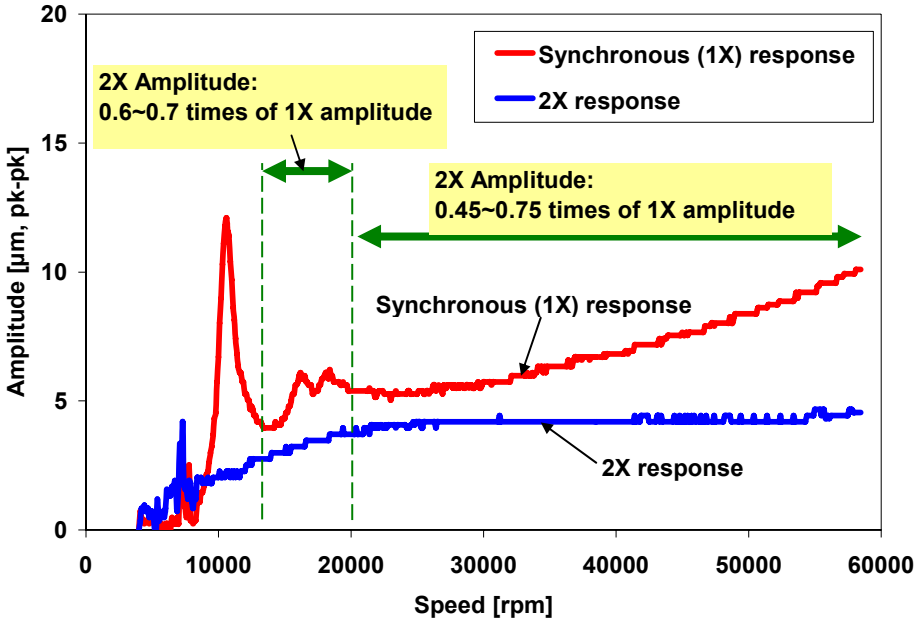

Fig. 13 Rotor synchronous (1X) and 2X responses versus rotor speed. 3.72 bar (ab) feed pressure into bearings. Measurements at rotor left end, horizontal plane (LH). Normal operation (w/o shocks).

Measurement of rotor motions due to impact excitations from the electromagnetic pusher

While coasting down from the top rotor speed of 60 krpm to rest, Figure 14 depicts time and rotor speed versus the impact forces applied to the test rig as delivered by the e-pusher. The direction of excitation is vertical against gravity. The measured amplitudes of impact forces vary between 100~400 N (pk-pk). Recall that the e-pusher is operated by a momentary push switch in an intermittent manner.

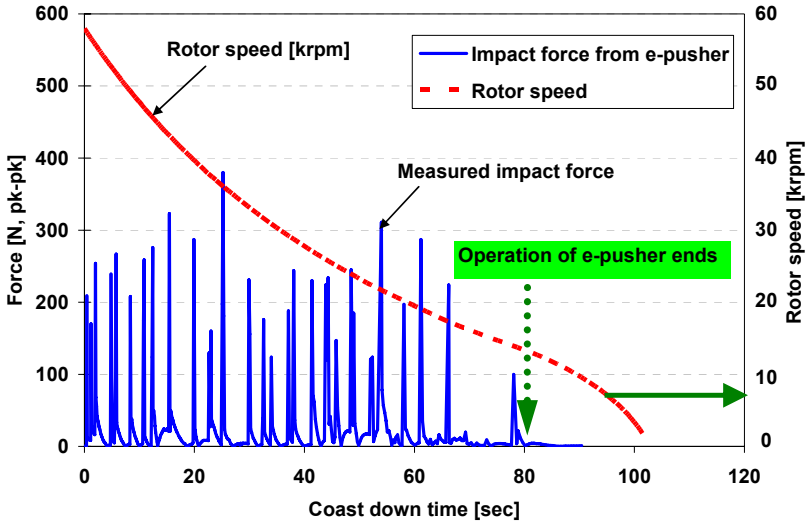

Fig. 14 Amplitude of impact load applied to rig base by e-pusher and rotor coast down speed versus time.

Under shock loads delivered from e-pusher, Figure 15 shows, at a rotor speed of 46 krpm, the measured typical accelerations of the test rig base plate and the left bearing housing and rotor response along the left end, horizontal direction (LH). Overall measured shock acceleration on the test rig base plate and bearing housing are ~15 g (pk-pk) and ~5 g (pk-pk), respectively [14] . The transient rotor response amplitude by these shock loads lasts approximately ~40 μm (pk-pk).

[14] The measured acceleration of the left bearing housing is ~35% of the acceleration of the base plate. When shock loads are applied to the test rig base, the assembling bolts and supporting stands may dissipate some of the impulsive energy. In addition, when the base plate hits the test table due to the rig lifting and dropping, the acceleration of (A2) is smaller than that of (A1) because the distance between the hinged fixture and (A2) is ~50% shorter than that between the hinged fixture and (A1). Thus, (A2) on the middle of the bearing housing records smaller impact accelerations than (A1) on the end of the base plate.

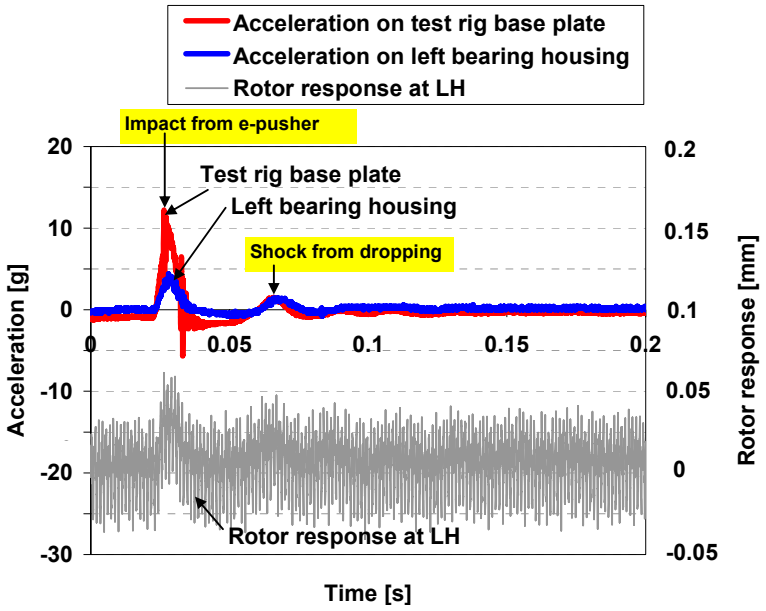

Fig. 15 Measured typical acceleration on test rig base plate and left bearing housing, and rotor displacement (LH) under shock loads delivered from e-pusher. 5.08 bar (ab) feed pressure into bearings. Rotor speed of 46 krpm.

As the rotor speed decreases from 60 krpm towards rest and while the e-pusher applies intermittent impacts to the test rig base, Figure 16 depicts a waterfall plot depicting the amplitude and frequency content of rotor motions. The measurement corresponds to 5.08 bar (ab) feed pressure condition. Rotor synchronous motions are dominant. Subsynchrous vibrations appear irregularly at a frequency of 200~250 Hz which corresponds with the system natural frequency[15]. The rotor amplitudes of subsynchrous motion are much smaller than those of synchronous motion, i.e., less than 10 % of synchronous rotor response amplitude.

[15] For 5.08 bar feed pressure, the critical speed of the rotor-bearing system at the rotor left end, horizontal plane is 12.1 krpm (200 Hz).

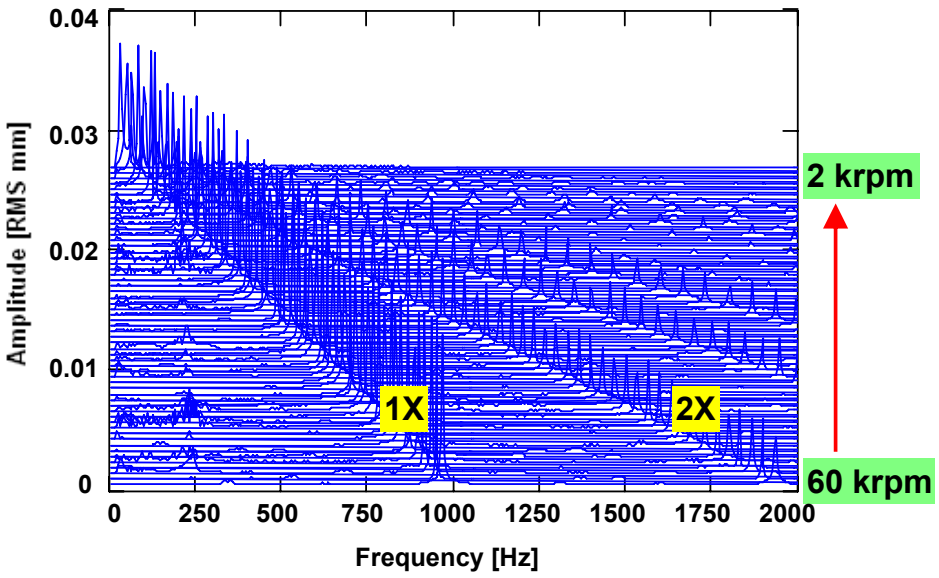

Fig. 16 Waterfall plot of rotor motions for test with 5.08 bar feed pressure. Measurements at rotor left and horizontal plane (LH). Impacts delivered with e-pusher.

Manual lift-drop tests

For the manual lift-drop tests, Figures 17 through 19 depict the recorded rotor amplitudes of overall and synchronous response, and overall shock pk-pk accelerations of the test rig base plate and left bearing housing. The overall rotor response amplitude increases remarkably under shock impacts over the entire speed range (60 ~10 krpm). The synchronous rotor responses for each pressure condition show significant fluctuations below 20 krpm, in particular around at speeds around the critical speed. Recall that the drop-induced impacts only excite motions in the frequency range below ~400 Hz, i.e., the synchronous (rotating) frequency is effectively isolated from the shock when the rotor spins above ~20 krpm. Therefore, above 20 krpm (beyond the critical speed), no notable difference appears in synchronous rotor responses compared with the responses when no shock impact is applied. Measured shock induced amplitudes of acceleration at the test rig base plate and bearing housing are 10~20 g (pk-pk) and 5~10 g (pk-pk), respectively, for each bearing feed pressure condition. The coast down rotor speed versus time, and shock load and rotor response amplitude in the time domain follow later.

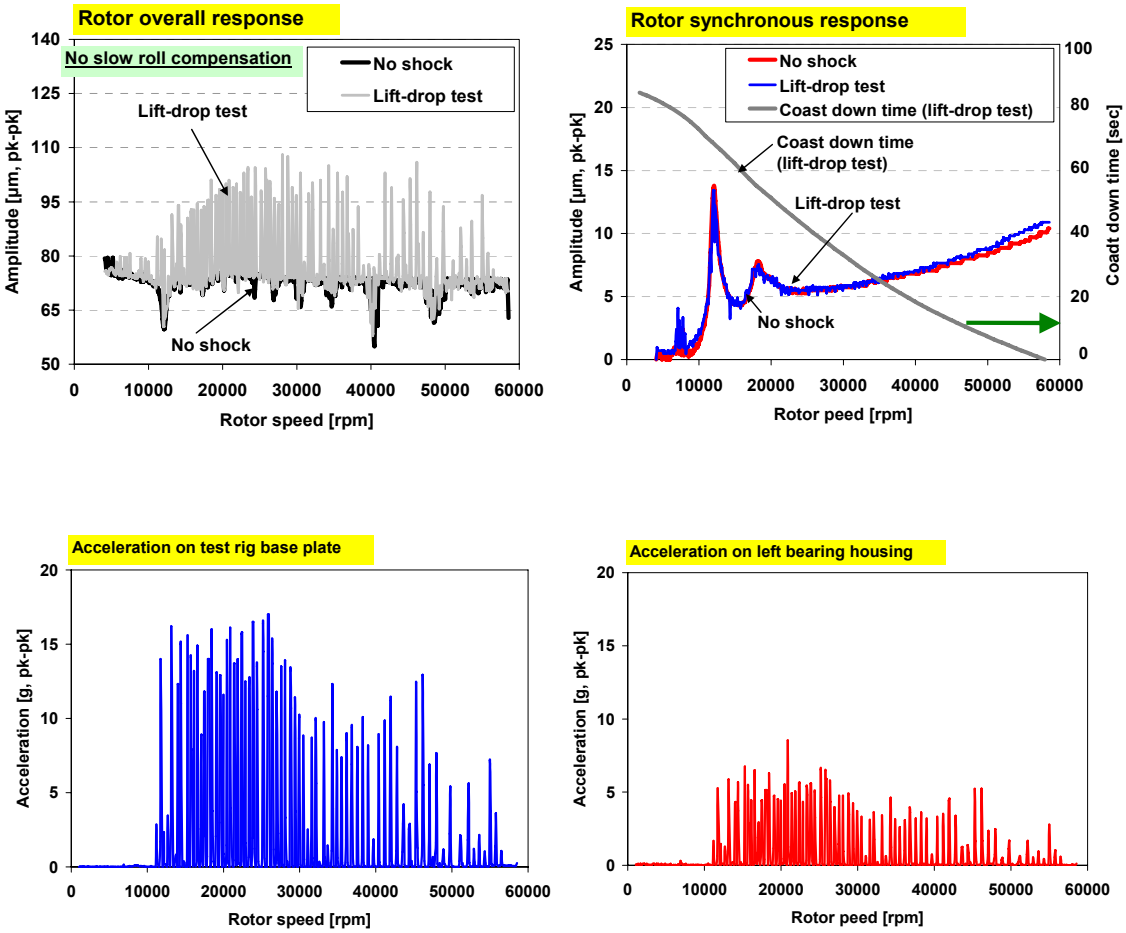

Fig. 17 Rotor synchronous response (rotor left end horizontal plane), shock pk-pk acceleration on the test rig base plate and bearing housing. 5.08 bar (ab) feed pressure into bearings. Manual lift-drop test.

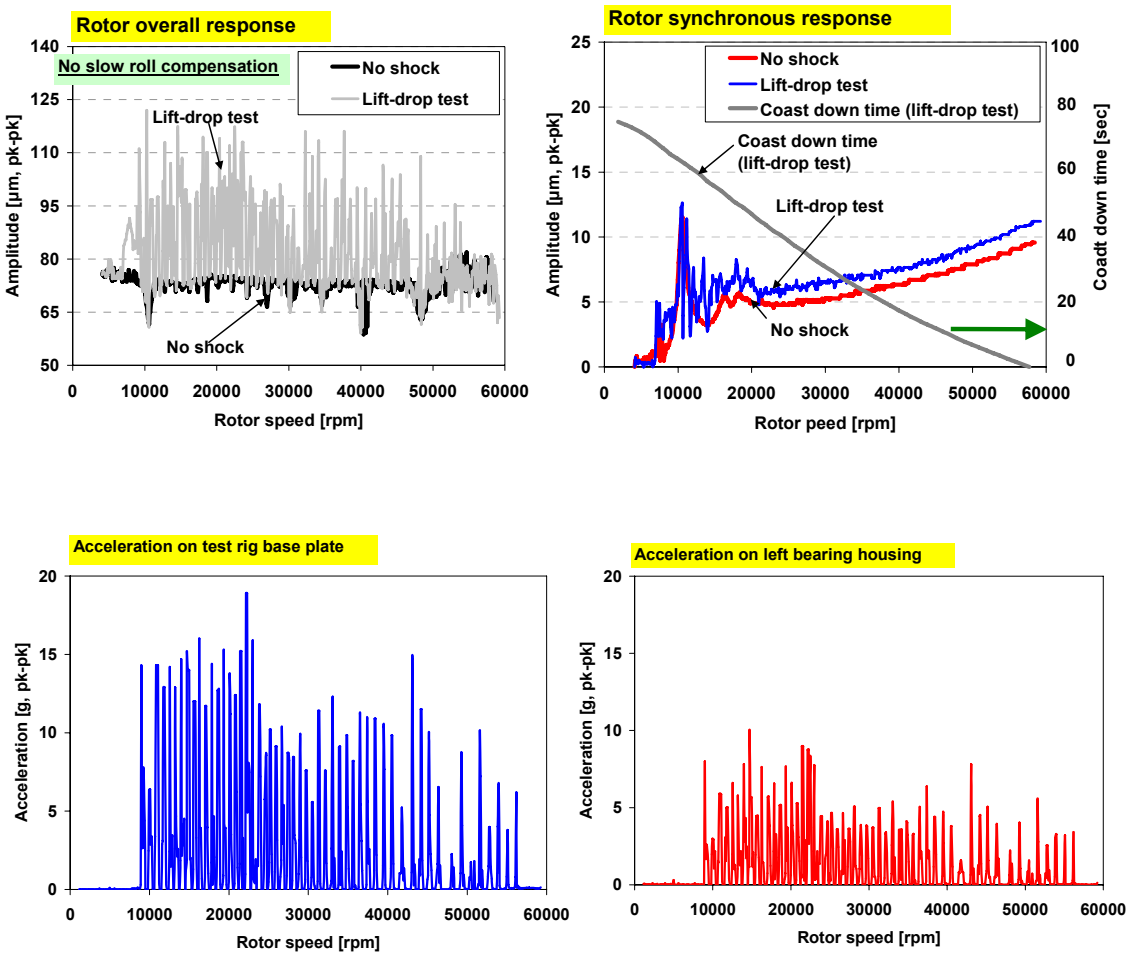

Fig. 18 Rotor synchronous response (rotor left end horizontal plane), shock pk-pk acceleration on the test rig base plate and bearing housing. 3.72 bar (ab) feed pressure into bearings. Manual lift-drop test.

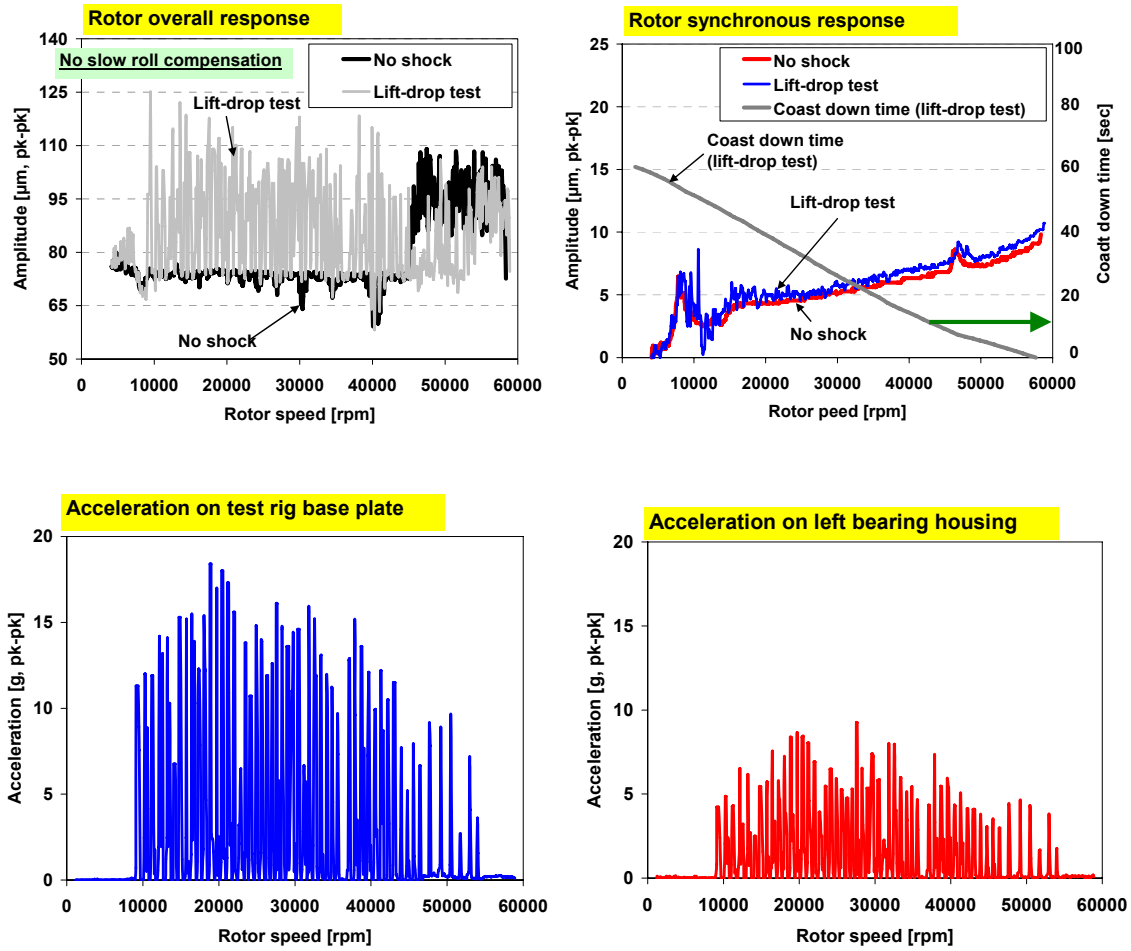

Fig. 19 Rotor synchronous response (rotor left end horizontal plane), shock pk-pk acceleration on the test rig base plate and bearing housing. 2.36 bar (ab) feed pressure into bearings. Manual lift-drop test.

For manual base tilt and drop tests, Figures 20 though 23 depict waterfall plots (amplitude and frequency content, and contour plots[16]) and synchronous and subsynchronous vibration amplitudes of rotor coast down tests recorded along the horizontal direction of the rotor left end (LH). The bearings are operated with 3.72 bar and 2.36 bar feed pressure, respectively. For 3.72 bar and 2.36 bar feed pressures into the bearing, subsynchronous vibrations appear over the entire coast down speed range because the shock excites the natural frequency of the rotor-bearing system. Overall amplitudes of subsynchronous rotor motion are of same order as synchronous vibration amplitudes. The system natural frequency

[16] In the waterfall contour plots of rotor displacement spectra, the amplitude of vibration is denoted by shades, with bright representing high levels and dark for low levels.

slightly increases with rotor speed [9, 33]. Subsynchronous frequencies, related to the natural frequency of the rotor-bearing system, are 185~220 Hz for 3.72 bar (ab) feed pressure and 150~180 Hz for 2.36 bar (ab) feed pressure. Additional subsynchronous frequencies, 30~40 Hz, become apparent at rotating speeds between 10~30 krpm and 20~40 krpm for 3.72 bar (ab) and 2.36 bar (ab) feed pressures, respectively. The subsychronous frequencies correspond closely with the natural frequency of the test rig components, see Appendix B.

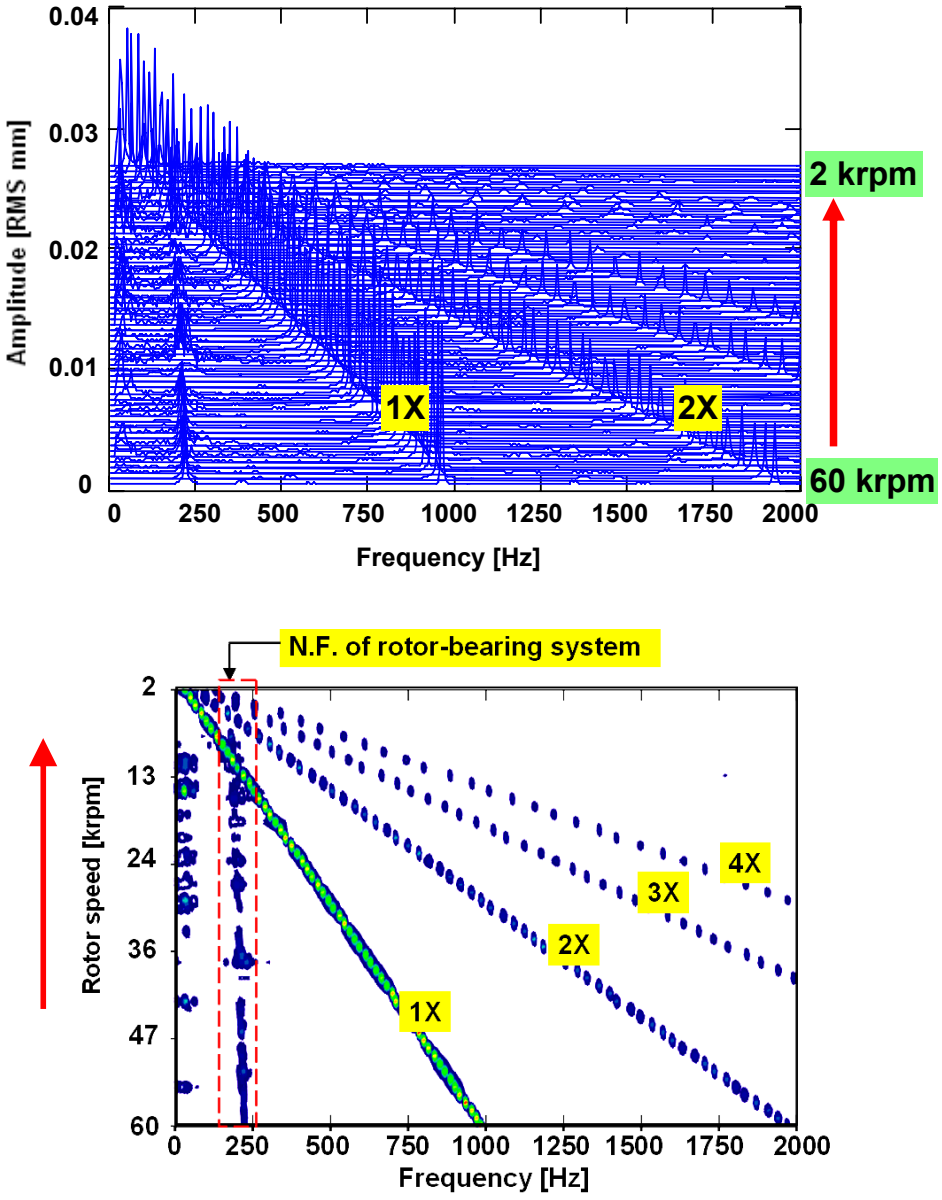

Fig. 20 Waterfall of rotor motions. 3.72 bar (ab) feed pressure. Lift-drop test. Measurements at rotor left end, horizontal plane (LH). N.F.: natural frequency.

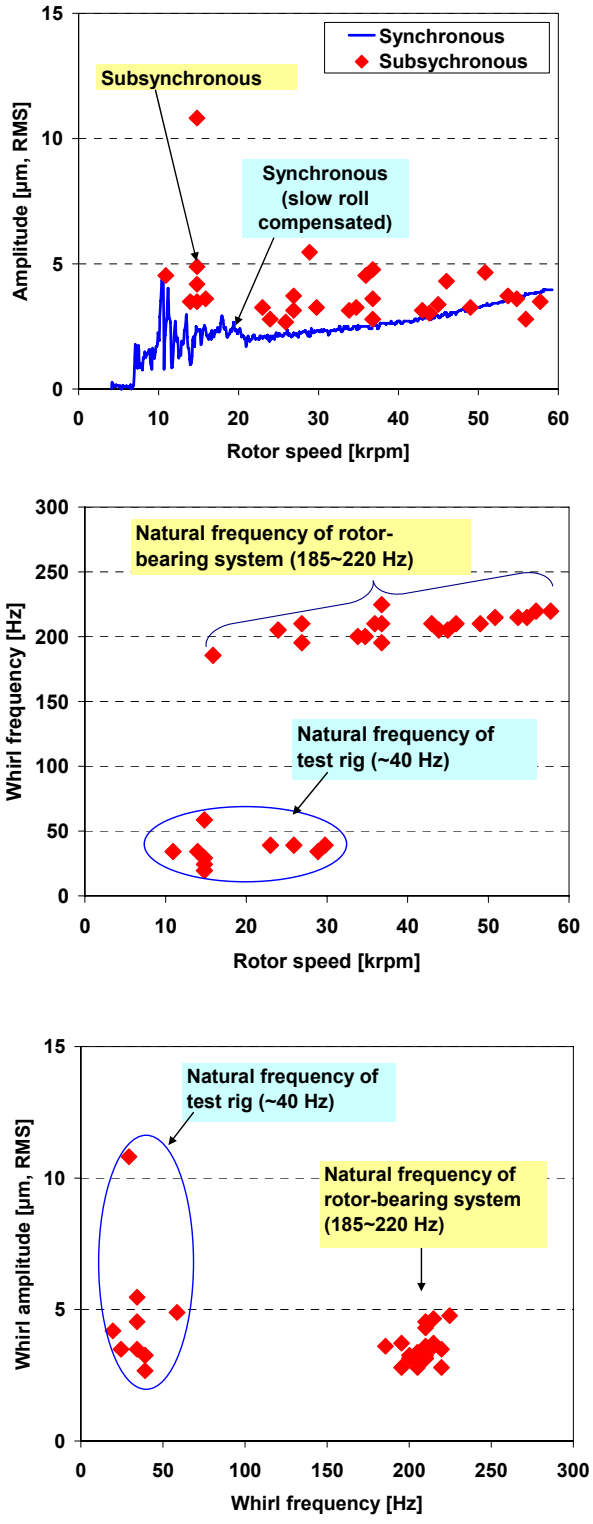

Fig. 21 Amplitude of synchronous and subsynchronous rotor motions. 3.72 bar (ab) feed pressure. Lift-drop test. Measurements at rotor left end, horizontal plane (LH).

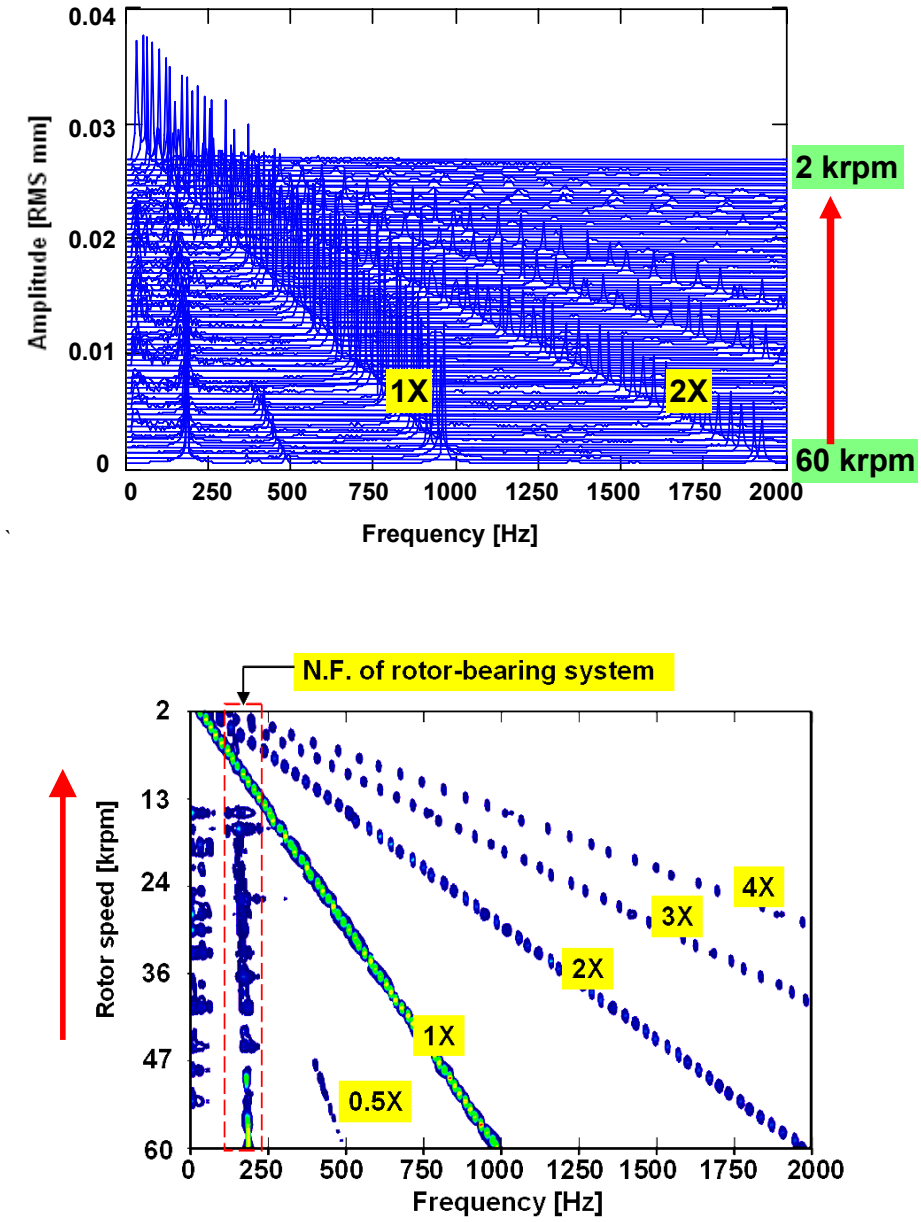

Fig. 22 Waterfall of rotor motions. 2.36 bar (ab) feed pressure. Lift-drop test. Measurements at rotor left end, horizontal plane (LH). N.F.: natural frequency.

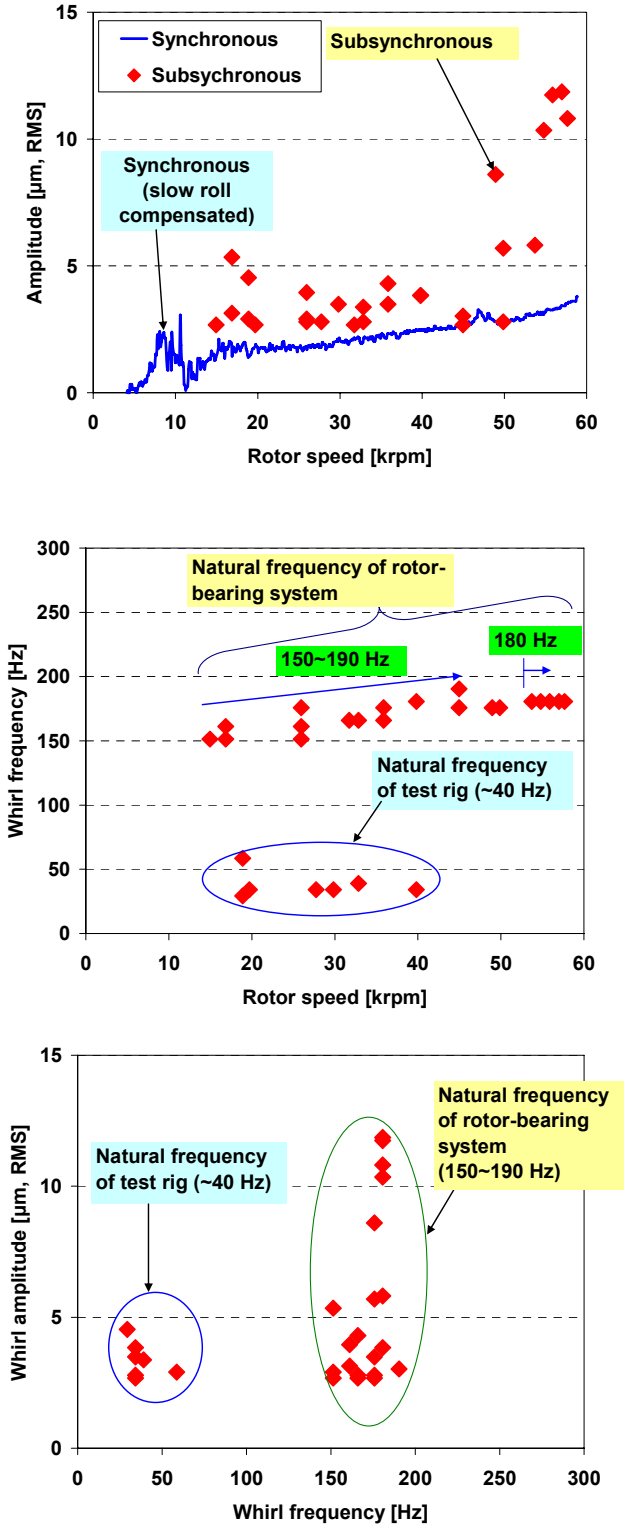

Fig. 23 Amplitude of synchronous and subsynchronous rotor motions. 2.36 bar (ab) feed pressure. Lift-drop test. Measurements at rotor left end, horizontal plane (LH).

From lift-drop tests, Figures 24 through 26 depict typical measured shock accelerations on the test rig base and the bearing housing, and the rotor displacements in the time domain for different rotor speeds and supply pressures into the bearings. Recall that the sampling size and rate are 2048 (2^{11}) and 10,000 samples/sec, respectively. The measured shock amplitude on the test rig ranges from 20 to 30 g (pk-pk) resulting from different drop heights[17]. After the test rig drops, the whole rig experiences multiple bounces. The rotor motions in these figures show raw displacement signals with shaft runout.

The rotor dynamic displacements over the entire operating speed range, even under shock levels of 20~30 g, are not excessive. The rotor transient responses are stable, and quickly returning to their before impact amplitude within 0.1 second. The post test inspection of the test rotor and bearings reveals no evidence of rotor and bearing contact. The test bearings show good tolerance to external shock and vibration with significantly high levels of damping even though the shock impacts are applied even when the rotor operates close to its critical speeds.

Appendix D shows predicted modal damping ratios of the test rotor-bearing system for an increasing feed pressure into the bearings. For increasing supply pressure conditions, the predicted damping ratios for the first and second rigid body modes range from 0.05 to 0.26.

[17] These shock loads are well above any that would be experienced during general driving or aircraft flight conditions [4, 14, 34].

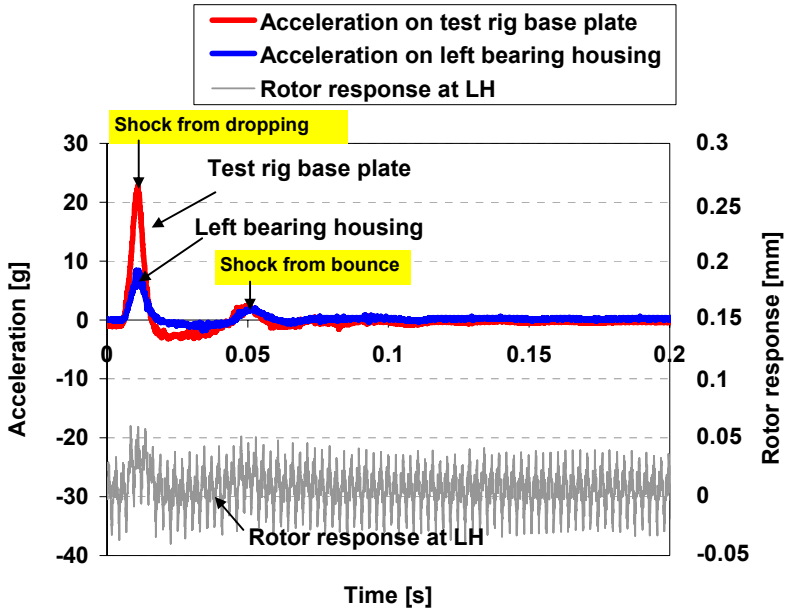

Fig. 24 Typical accelerations of test rig base plate and left bearing housing, and rotor response (LH). Lift-drop test. 5.08 bar (ab) feed pressure into bearings. Rotor speed of 23 krpm.

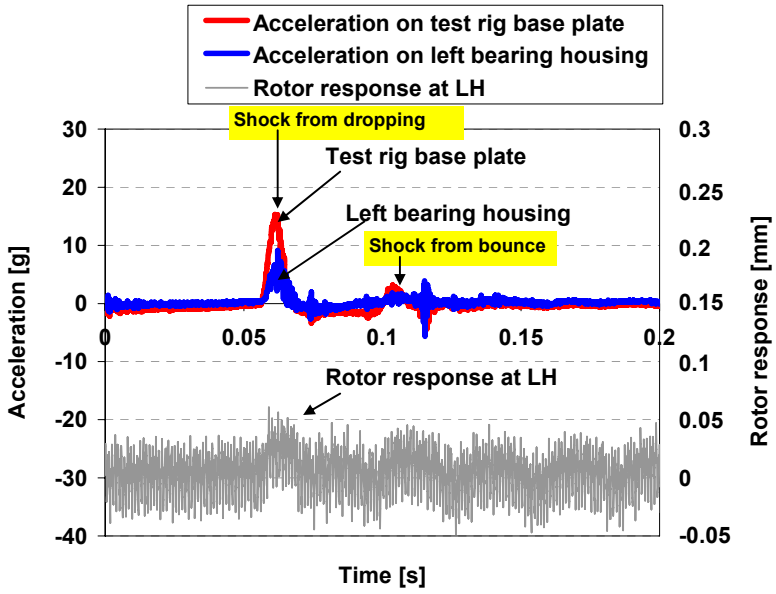

Fig. 25 Typical accelerations of test rig base plate and left bearing housing, and rotor response (LH). Lift-drop test. 3.72 bar (ab) feed pressure into bearings. Rotor speed of 53 krpm.

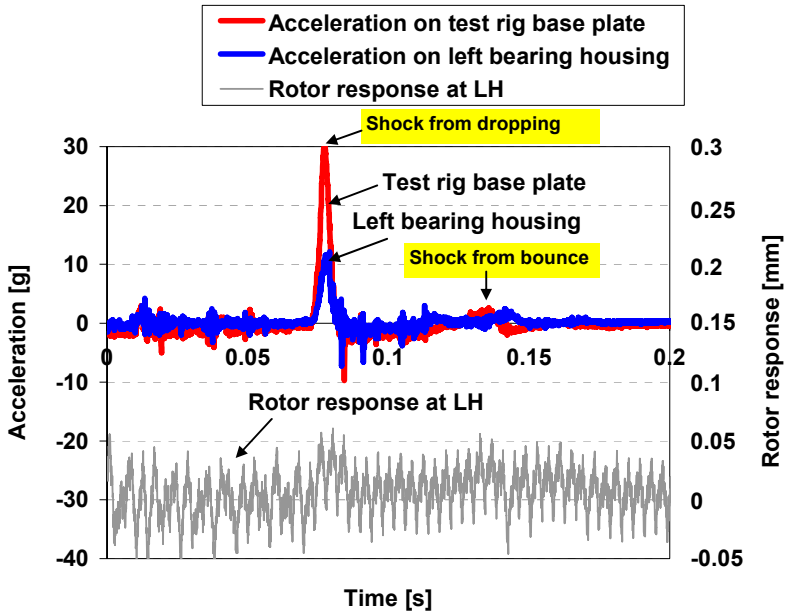

Fig. 26 Typical accelerations of test rig base plate and left bearing housing, and rotor response (LH). Lift-drop test. 2.36 bar (ab) feed pressure into bearings. Rotor speed of 15 krpm.

Coast down rotor speed and type of drag

Figure 27 depicts the recorded coast down rotor speed versus time for increasing supply pressures into the test bearings when no shock impacts are applied. The time for the rotor to coast down is over 80 seconds which denotes very low air drag operation (nearly friction free). A 3.72 bar (ab) or a 5.08 bar (ab) feed pressure into the bearings produces almost identical rotor coast down speed curves versus time. The rotor coast down speed curves for 2.36 bar (ab) feed pressure shows a rapid deceleration from a top seed (60 krpm) to 45 krpm, and corresponds with the onset speed of significant subsynchronous vibration, see Figure 12.

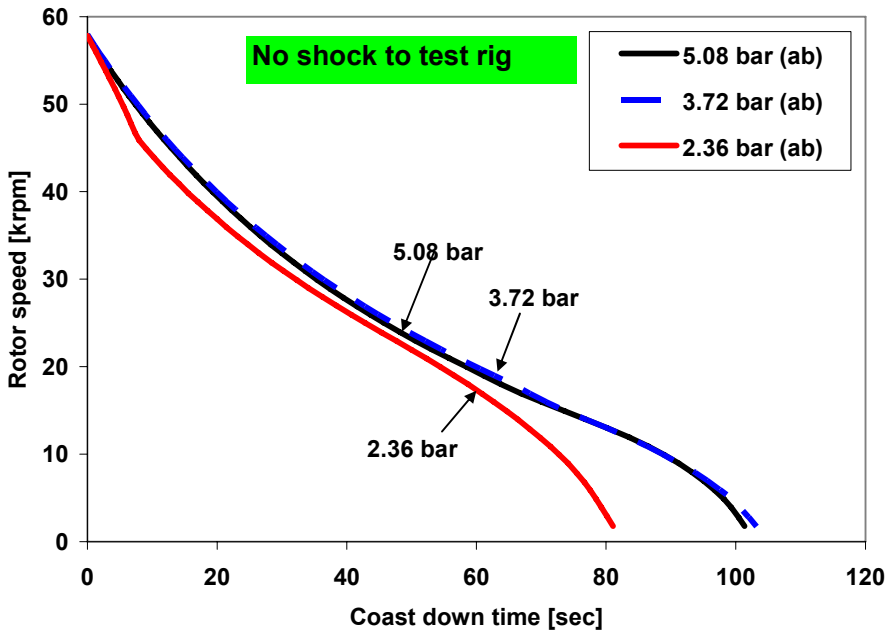

Fig. 27 Recorded rotor coast down speed versus time for operation of bearings with increasing supply pressures. Normal operating (no shock) test.

For the gas bearings supplied with 5.08 bar feed pressure, Figure 28 depicts the rotor coast down speed curves versus time for the test conditions of no shock, e-pusher, and lift-drop tests. There is no significant difference in rotor coast down time for cases with impacts from e-pusher and no shock conditions. The results reveal an exponential decay of rotor speed with time from 60 krpm to ~10 krpm. From 10 krpm until rest, rotor operation shows dry friction effects (rubbing between the test rotor and its bearings) with a fast deceleration to rest. Overall coast down time for the lift-drop test is ~15 second shorter than that due to the e-pusher excitation or no shock tests. Note that the applied shock amplitudes and frequencies to the test system do not affect notably the rotor touch down speed (~10 krpm with and without shock conditions).

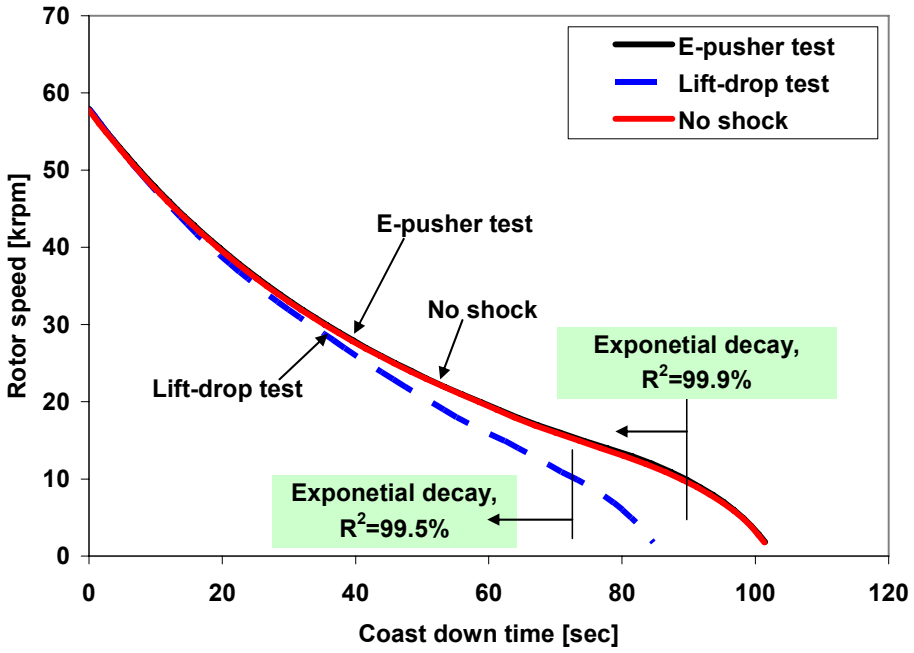

Fig. 28 Coast down rotor speed versus time. No shock, e-pusher, and lift-drop tests. 5.08 bar (ab) feed pressure into bearings.

Figure 29 shows the coast down speed versus time for the lift-drop tests for three conditions of supply pressure into the bearings. The figure also displays the shock amplitude versus coast down time. For each supply pressure condition, the overall coast down time reduces remarkably with drop-induced shock loads. Notice that even though the test rotor-bearing system is subjected to severe external shock loads, the rotor coast down curves shows a decaying exponential shape. The calculated R^2 of an exponential decay renders a goodness of correlation of 98~99%. The exponential decay in coast down speed is typical of a rotating system with viscous drag, and hence demonstrates no contact between the rotor and bearings' surfaces.

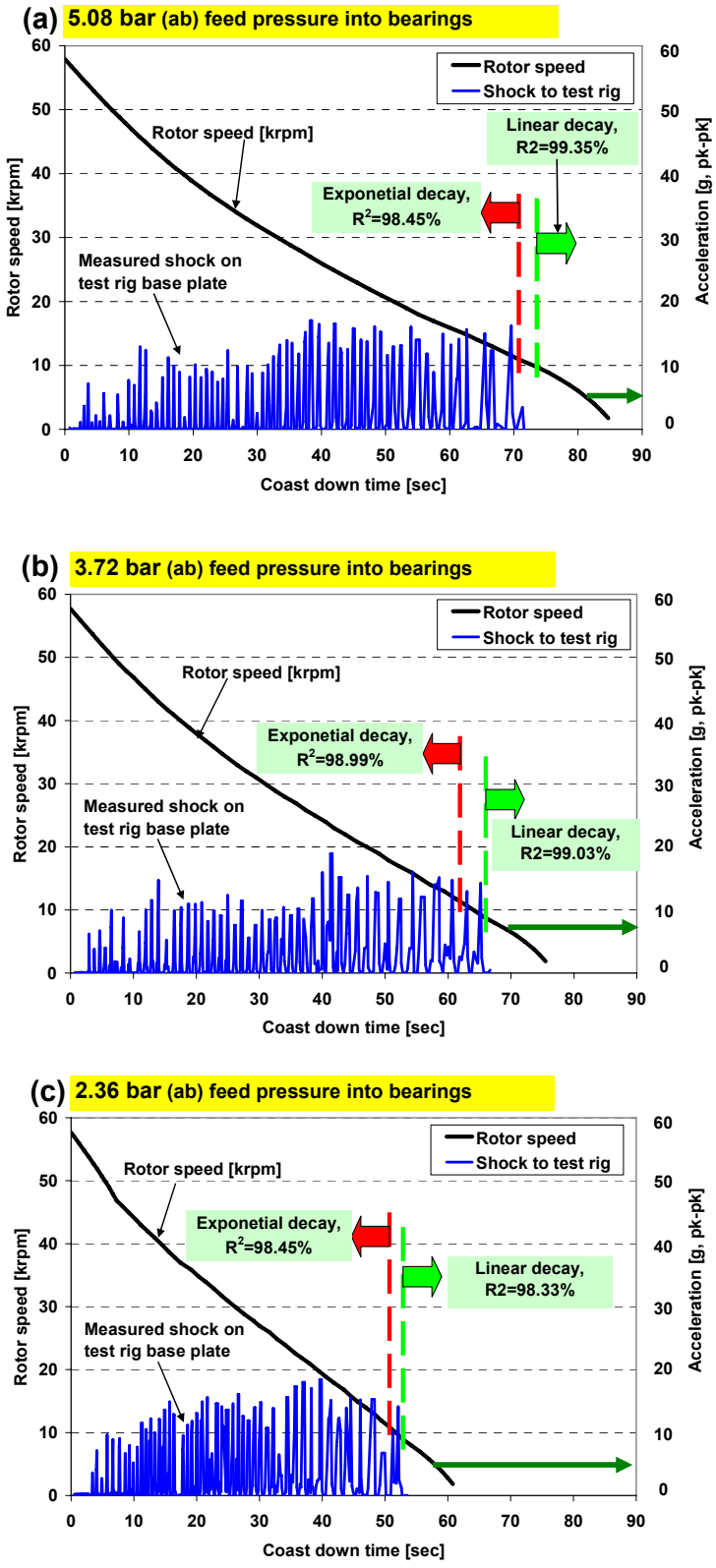

Fig. 29 Measured shock loads on test rig base and rotor coast down speed versus time. Lift-drop tests. Feed pressure into bearings equal to (a) 5.08 bar (b) 3.72 bar (c) 2.36 bar.

Conclusions

Experiments on a rotor-hybrid gas bearing system are performed under intermittent shocks on its base. Two flexure pivot tilting pad hydrostatic gas bearings support the test rotor, 0.825 kg and 28.6 mm in diameter. The test bearings comprise four arcuate 72° pads, offset 60 %, and 0.6 mm feeding holes in each pad. From prior extensive testing [9, 23, 24], the gas bearings have uneven pads surface thereby rendering dissimilar clearance along the axial and circumferential directions.

Two excitation methods are used to apply shock loads to the test rig: 1) delivering impacts to the rig base via an electromagnetic pusher (i.e., e-pusher test), and 2) hand lifting one end of the rig base and dropping it (i.e., lift-drop test). The e-pusher is installed under the support table to apply shock loads to the test rig base plate. Rotor speed deceleration tests from 60 krpm are conducted to characterize the rotor dynamic response during normal operation (w/o shock) and shock loads tests. The impact forces from the e-pusher tests and manual lift-drop tests render intermittent shocks to the whole test system and excite frequencies below ~400 Hz. The applied shock loads range between 5~10 g and 5~30 g (pk-pk) for the e-pusher tests and the lift-drop tests, respectively.

Under shock impacts, for each pressure condition, the overall rotor response amplitude increases significantly and the synchronous rotor response at speeds around the system critical speeds show significant fluctuations. For the gas bearings supplied with 3.72 bar and 2.36 bar (ab), notable subsynchronous vibrations, related to the natural frequency of the rotor-bearing system, appear over the entire coast down speed range. Note that the subsynchronous rotor vibration under shock loads condition is not a gas bearing rotordynamic instability but an excitation of the system natural frequency induced by the shock. Excitation of an additional subsynchronous frequency, corresponding to the test rig fundamental natural frequency, also becomes apparent.

For each feed pressure condition into the bearings, the rotor transient response amplitudes under severe shock loads condition, as high as ~30 g (pk-pk), do not exceed ~50 μm (pk-pk) and restore to their before impact amplitude within 0.10 second. The overall rotor coast down time decreases notably with drop-induced shock loads. The decay of rotor speed is of exponential type which indicates viscous drag effects are dominant for most of the operating speed range, i.e., no contact between the rotor and bearing surfaces.

The shock loads applied in the current tests, up to ~30 g (pk-pk) are well above any that would be experienced during general vehicle driving or aircraft flight conditions [4, 14, 34].

The current work delivers further reliable experimental data on the rotordynamic performance of a rotor-gas bearing system addressing to the robustness of test hybrid gas bearings to intermittent and severe external shocks.

References

[1] Valco, M. J., and DellaCorte, C., 2002, "Emerging Oil-Free Turbomachinery Technology for Military Propulsion and Power Applications," *Proc. 23rd U.S. Army Science Conference*, Fort Lauderdale, FL.

[2] San Andrés, L, and Kim, T. H., 2008, "Forced Nonlinear Response of Gas Foil Bearing Supported Rotors," Tribo. Int., In Press

[3] San Andrés, L., 2007, "Gas Bearings for Oil-free Turbomacinery-Identification of Force Coefficients from Impact Loads," Proposal to TAMU Turbomachinery Research Consortium, Texas A&M University, College Station, TX.

[4] Heshmat, H., and Walton, J. F., 2000, "Oil-Free Turbocharger Demonstration Paves Way to Gas Turbine Engine Applications," ASME paper 2000-GT-620.

[5] Larue, G. D., Kang, S. G., and Wick, W., 2006, "Turbocharger with Hydrodynamic Foil Bearings," United States Patent, No.7,108,488 B2.

[6] Breedlove, A., 2007, "Experimental Identification of Structural Force Coefficients in a Bump-Type Foil Bearing," Texas A&M University, M.S. Thesis, College Station, TX.

[7] Kim, T.H., 2007, "Analysis of Side End Pressurized Bump Type Gas Foil Bearings: A Model Anchored To Test Data," Ph.D. Dissertation, Texas A&M University, College Station, TX.

[8] San Andrés, L., 2006, "Hybrid Flexure Pivot-Tilting Pad Gas Bearings: Analysis and Experimental Validation," ASME J. Tribo., **128**, pp. 551-558.

[9] San Andrés, L., and Ryu, K, 2008, "Flexure Pivot Tilting Pad Hybrid Gas Bearings: Operation With Worn Clearances and Two Load-Pad Configurations," ASME J. Eng. Gas Turbines Power, **131**, 042506.

[10] Hamrock, B. J., 1994, *Fundamentals of Fluid Film Lubrication*, McGraw-Hill, New York.

[11] Zhang, Q., Guo, G., and Bi, C., 2005, "Air Bearing Spindle Motor for Hard Disk Drives," STLE Tribol. Trans., **48**, pp. 468-473.

[12] Spencer, P. R., Curwen, P. W., and Tryon, H. B., 1971, "Effect of Vibration and Shock on the Performance of Gas Bearing Turbomachinery, I- Half-Sine Shock and Sinusoidal Vibration," NASA-CR-1762

[13] Tessarzik, J. M., Chiang, T., and Badgley, R. H, 1974, “The Response of Rotating Machinery to External Random Vibration,” ASME J. Eng. Indus., **96**, pp. 477-489.

[14] Walton, J. F., Heshmat, H., and Tomaszewsky, M. J., 2008, “Testing of a Small Turbocharger/Turbojet Sized Simulator Rotor Supported on Foil Bearings,” ASME J. Eng. Gas Turbines Power, **131**, 035001.

[15] Walton, J. F., and Heshmat, H., 2002, "Application of Foil Bearings to Turbomachinery Including Vertical Operation," ASME J. Eng. Gas Turbine Power, **124**, pp. 1032-1041.

[16] Hori, Y, Kato, T., 1992, “Earthquake-Induced Instability of a Rotor Supported by Oil Film Bearings,” ASME J.Vib. Acoust., **112**, pp.160–165.

[17] Suarez, L. E., Singh, M. P., Rohanimanesh, M.S., 1992, “Seismic Response of Rotating Machines,” Earthquake Eng. Struct. Dyn, **21**, pp. 21–36.

[18] Gaganis, B. J., Zisimopoulos, A. K., Nikolakopoulos, P. G., Papadopoulos, C. A., 1999, “Modal Analysis of Rotor on Piecewise Linear Journal Bearings Under Seismic Excitation,” ASME J. Vib. Acoust., **121**, pp. 190–196.

[19] Subbiah, R., Bhat, R. B., and Sanker, T. S., 1985, "Response of Rotors Subjected to Random Support Excitations," ASME J. Vib. Acoust. Stress Reliab. Design, **107**, pp. 453-459.

[20] Lee, A. S., Kim, B. O., and Kim, Y. -C., 2006, “A Finite Element Transient Response Analysis Method of a Rotor-Bearing System to Base Shock Excitation Using the State-Space Newmark Scheme and Comparisons with Experiments,” J. Sound Vib., **297**, pp. 595-615.

[21] Lee, A. S., and Kim, B. O., 2007, “A FE Transient Response Analysis Model of a Flexible Rotor-Bearing System With Mount System To Base Shock Excitation,” ASME paper GT2007-27677.

[22] Duchemin, M., Berlioz, A., Ferraris, G., 2006, "Dynamic Behavior and Stability of a Rotor Under Base Excitation," ASME J. Vib. Acous., **128**, pp. 576-585.

[23] San Andrés, L, Ryu, K., 2008, "Hybrid Gas Bearings with Controlled Supply Pressure To Eliminate Rotor Vibrations While Crossing System Critical Speeds," ASME paper GT2008-50393. ASME J. Eng. Gas Turbines Power (to be published)

[24] Zhu, X., and San Andrés, L., 2007, “Rotordynamic Performance of Flexure Pivot Hydrostatic Gas Bearings for Oil-Free Turbomachinery,” ASME J. Eng. Gas Turbines Power, **129**, pp. 1020-1027.

[25] Wojtecki, R. G, 1999, *Air Logic control for automated systems*, CRC Press, Boca Raton, FL.

[26] Bently Nevada LLC, 2007, "ADRE® for Windows®/DAIU, Bently NevadaTM Asset Condition Monitoring," Specifications and Ordering Information, Part Number 141577-01, Rev. F, Minden, Nevada.

[27] Harris, C. M., 1995, *Shock and Vibration Handbook*, McGraw-Hill, NY.

[28] Silva, D. W., 2007, *Vibration Monitoring, Testing, and Instrumentation*, CRC Press, Boca Raton, FL.

[29] Lalanne, C., 2002, *Mechanical Shocks*, Hermes Penton Ltd, London.

[30] Bently, D.E., 2002, *Fundamentals of Rotating Machinery Diagnostic*s, Bently Pressurized Bearing Company, Minden, NV.

[31] Peirs, J.,Waumans, T., Vleugels, P., Al-Bender, F., Stevens, T.,Verstraete, T., Stevens, S., D'hulst, R., Verstraete, D., Fiorini, P., Braembussche, R., Driesen, J., Puers, R., Hendrick, P., Baelmans, M.., and Reynaerts, D., 2007, "Micropower Generation With Microgasturbines: a Challenge," *Proc. IMechE Part C: J. Mechanical Engineering Science*, **221**, pp. 489-500.

[32] Pennacchi, P., and Frosini, L., 2005, "Dynamical Behaviour of a Three-phase Generator Due to Unbalanced Magnetic Pull," *IEE Proc. Electr. Power Appl.*, **152**, pp. 1389-1400.

[33] Ryu, K., 2007, "Hybrid Gas Bearings with Controlled Supply Pressure to Eliminate Rotor Vibrations While Crossing System Critical Speeds," Masters thesis, Texas A&M University, College Station, TX.

[34] Wei, X., 2004, "Modeling and Control of a Hybrid Electric Drivetrain for Optimum Fuel Economy, Performance, and Driveability," Ph.D. Dissertation, Ohio State University, Columbus, OH.

[35] San Andrés, L., and Ryu, K., 2006, "Test Results for Load-On-Pad and Load-Between-Pad Hybrid Flexure Pivot Tilting Pad Gas Bearings," TL-B&C-1-06, Turbomachinery Laboratory Research Report, Texas A&M University, College Station, TX.

Appendix A. Estimated bearing radial clearances

Prior extensive testing with the bearings [9, 23, 24] left the pads' surfaces with uneven wear. Presently, the test bearings have quite dissimilar clearances along the circumference and axial directions of each bearing pad. Note that the original bearing nominal clearance and dimensionless pad preload are 40±4.5 μm and 40%, respectively [24].

The bearing radial clearance (C_b) is estimated by subtracting the measured rotor diameter from the measured bearing diameter (D_b). Figure A.1 depicts presently estimated bearing radial clearances on the test bearings, and a comparison with prior measurements [33]. The estimated radial clearances vary from 40~90 μm for the left bearing and 30~70 μm for the right bearing.

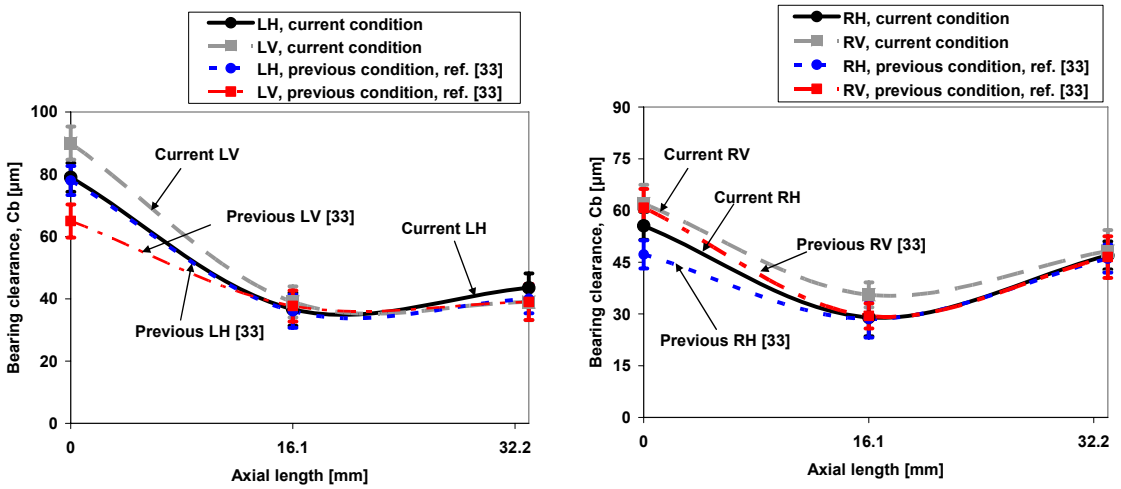

(a) Left bearing (b) Right bearing

Fig. A.1 Estimated bearing radial clearances of left (L) and right (R) bearings along horizontal (H) and vertical (V) directions.

Appendix B. Measured natural frequencies of test rig

Impact tests are conducted to determine the natural frequencies of the test rig. Figure B.1 depicts a schematic view of the test rig, accelerometer locations, and impact location. An instrumented impulse hammer (2.5 lb hammer with force sensor[18] and inertia mass) delivers impact loads to the test rig base. A soft rubber tip is used on the hammer head to excite low frequencies of the test rig. By switching the location of the accelerometer[19] from positions 1 through 4, the natural frequencies of the test rig main body (comprised of the housings for left bearing, right bearing, and motor) and base plate are measured. The test procedure includes five repetitions of the impact excitation for each measured position. An average process in the frequency domain is performed.

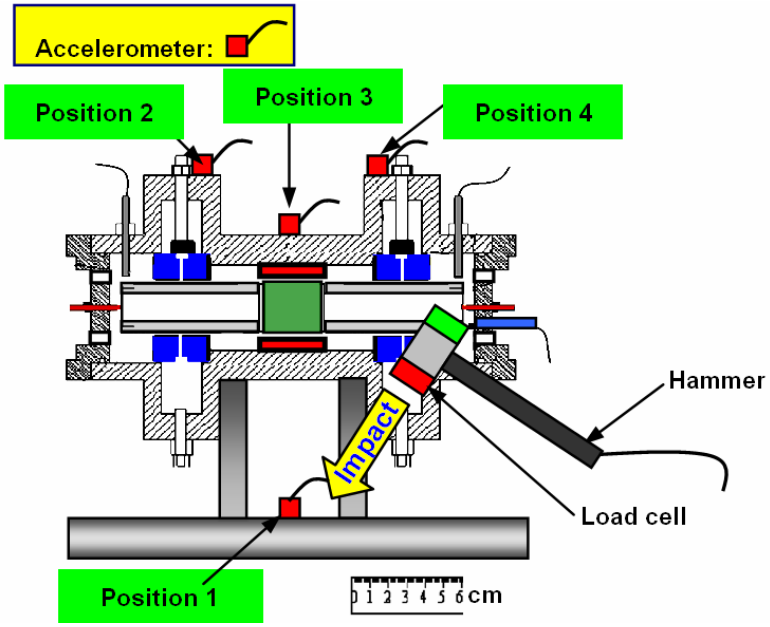

Fig. B.1 Schematic view of impact test and measurement positions of acceleration under impact force.

Figure B.2 shows a typical impact force from the impact hammer[20]. The maximum force from the impact hammer is ~550 N (pk-pk) and the excited frequency range does not exceed 300 Hz because of the hammer's soft tip.

[18] The sensitivity of the load cell is 0.23 mV/N.
[19] The sensitivity of the accelerometer (A1) is 5mV/g.
[20] The shock loads from the e-pusher and lift-drop tests render multiple intermittent impacts to the test rig. However, this impact hammer only delivers single impact force to the test rig.

For the sensor atop the left bearing housing (sensor position 2), Figure B. 3 displays the recorded acceleration due to the excited impact. The peak amplitude appears at 40 Hz. The estimated damping ratio, calculated from the Q-factor method, for this frequency is ~10%.

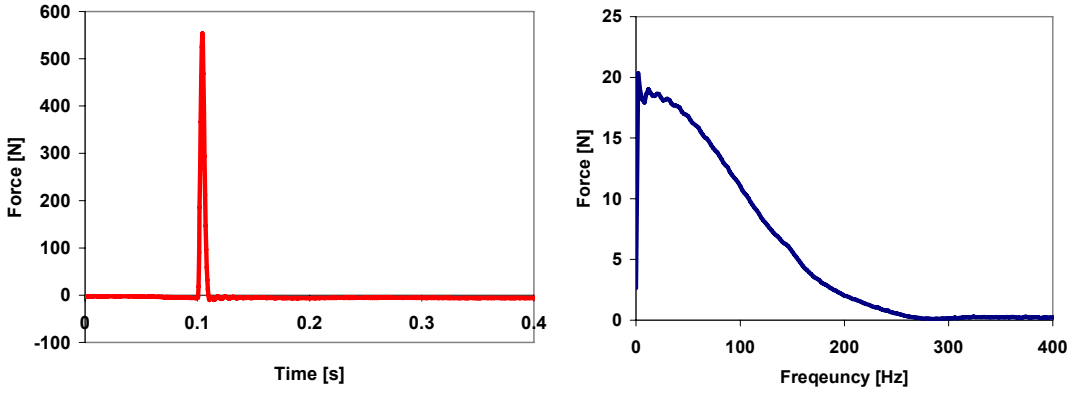

Fig. B.2 Typical time signal and frequency spectrum of impact force from impact hammer. Pre-trigger 0.1 second.

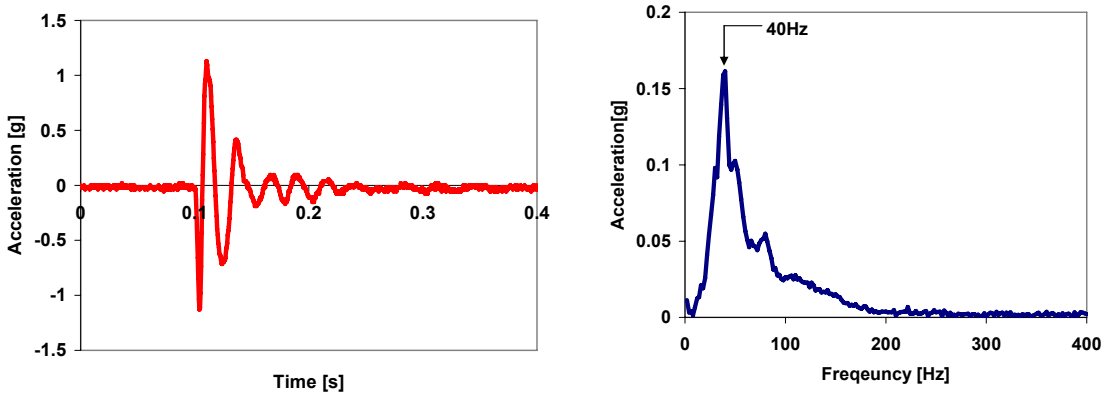

Fig. B.3 Typical time signal and frequency spectrum of acceleration atop left bearing housing (sensor position 2) under single impact (Fig. B.2). Pre-trigger 0.1 second.

Figure B. 4 depicts the measured acceleration for positions 1 through 4 due to the impact force. The distinctive peak amplitude at ~40 Hz renders the fundamental natural frequency of the test rig.

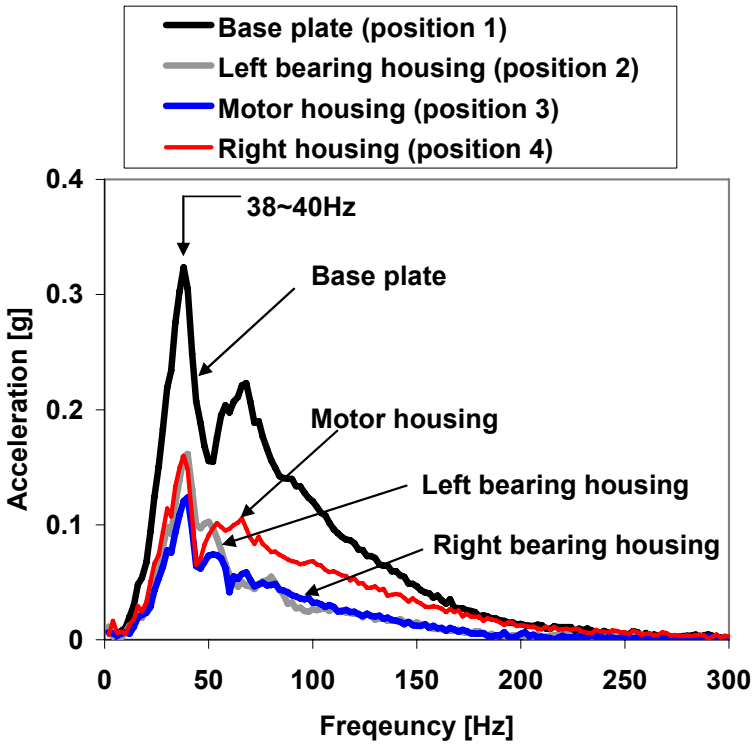

Fig. B.4 Frequency spectra of acceleration on test rig base plate (position 1), atop left bearing (position 2), atop right bearing (position 4), and motor body (position 3) due to impacts on base (Fig. B.2). Measurement locations depicted in Fig. B.1.

Appendix C. Obtained rotordynamic parameters of test rotor-bearing system from normal operation tests

For no shock tests, Figure C.1 depicts the amplitudes of rotor synchronous motions measured at the rotor left end, horizontal plane (LH). The supply pressures into the bearings are 2.36 bar, 3.72 bar, and 5.08 bar (ab). External pressurization into the test bearings increases their direct stiffnesses, thereby rising the system critical speed.

The rotor amplitudes of synchronous motion steadily increase with rotor speed due to the peculiar imbalance distribution of the test rotor detailed in Appendix. D. Note that the measured first free-free natural frequency (bending mode) of the test rotor is 1.92 kHz (115 krpm) thus the rotor can be regarded as rigid over the test speed range (<60 krpm) [35].

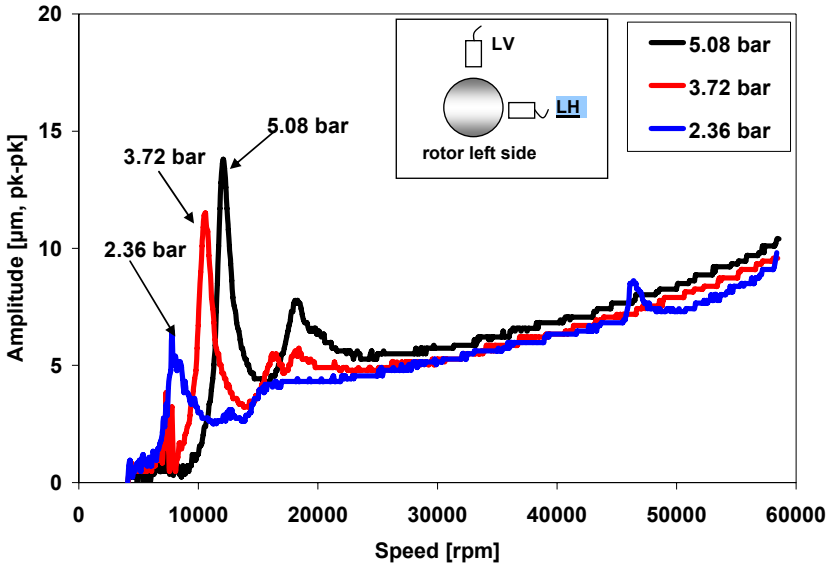

Fig. C.1 Amplitude of synchronous response versus rotor speed for increasing feed pressure. Measurements at rotor left end, horizontal plane (LH). Normal operation (No shock).

Table C.1 shows the estimated effective bearing stiffness coefficients and damping ratios determined from the baseline imbalance responses with various supply gas pressures. The effective stiffness coefficient (K_{eff}) is determined from the system critical speed, i.e., $K_{eff}=\omega_c^2 m$. Note that m is the rotor mass shared by each bearing. The Q factor method is used to estimate the viscous damping ratio (ζ) of the rotor on its bearings. The magnitudes of

critical speed along each measurement direction increase linearly with feed pressure. The damping ratios decrease as the supply pressure increases.

Table C.1 Estimated equivalent stiffness and damping ratio for gas bearings derived from rotor imbalance response at system critical speeds

Displacement sensor	Supply absolute pressure [bar]	Critical speed [rpm]	Effective stiffness [MN/m]	Damping ratio
LV	5.08	11.7	0.619	0.038
	3.72	10.2	0.470	0.054
	2.36	7.1	0.227	*[21]
LH	5.08	12.1	0.662	0.041
	3.72	10.6	0.508	0.049
	2.36	7.8	0.275	0.067
RV	5.08	18.8	1.597	0.057
	3.72	16.8	1.275	0.065
	2.36	13.3	0.799	0.116
RH	5.08	17.4	1.368	0.075
	3.72	15.2	1.044	0.108
	2.36	12.1	0.662	*

Uncertainty of critical speed: 100 rpm

[21] *The displacement peak amplitude is not evident (multiple peaks as well as too broad) to identify a critical speed.

Appendix D. Rotordynamic analysis of test rotor-bearing system during normal operation (without shock loads)

The rotordynamic analysis consists of modeling the test rotor structure with **XLTRC^2®** and predicting the gas bearing force coefficients with **TILTPADHGB©,** developed by San Andrés [8]. Reference [35] details the test rotor FE structural model.

In the bearing predictive model, the representative radial clearances (C_p=R_p-R_j) and preload are 38 μm and 7.2 μm for the right bearing and 45 μm and 5.4 μm for the left bearing, respectively[22].

Figure D.1 depicts the measured and predicted bearing mass flow rates versus supply pressure[23]. A larger clearance on the left bearing determines a higher flow rate than for the right bearing. A smaller flow rate indicates smaller film pressures acting on the bearing at the orifice location. Imperfect sealing of the feed pressure chamber for the left bearing causes discrepancies between the measured and predicted mass flow rates.

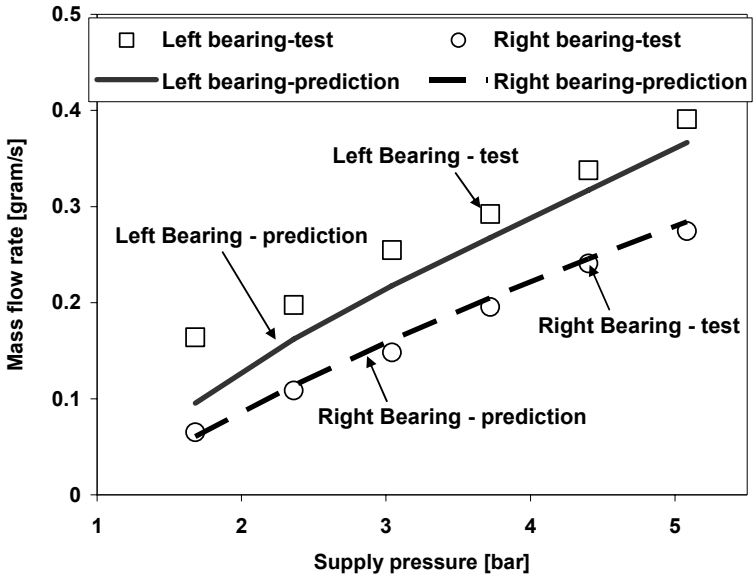

Fig. D.1 Measured and predicted mass flow rates for test bearings versus supply pressure.

[22] The dimensionless pad preloads for the previous tests in [23] are 0.22 for the right bearing and 0.15 for the left bearing. Note that the radial clearances and preloads used in bearing predictive model are representative only.

[23] Calibrated turbine flow meters (uncertainty: 0.05 Liter/min) measure the mass flow rate into each bearing.

Predicted (synchronous) force coefficients for each supply pressure condition are incorporated into **XLTRC^2®** for prediction of the rotor imbalance response. The eigenvalue analysis of the rotor-bearing system renders the natural frequencies and modal damping ratios.

Figure D.2 depicts the predicted damped natural frequency of the test rotor-bearing system for 5.08 bar bearing feed pressure. The predicted critical speeds are in agreement with those measured. Figure D.3 shows first two rigid body (conical[24]) modes, corresponding with the system critical speeds at 13 krpm and 17 krpm shown in Figure D.2. Figure D.4 depicts the predicted modal damping ratios for increasing feed pressures into the bearings. As the supply pressure increases, the modal damping ratios decrease.

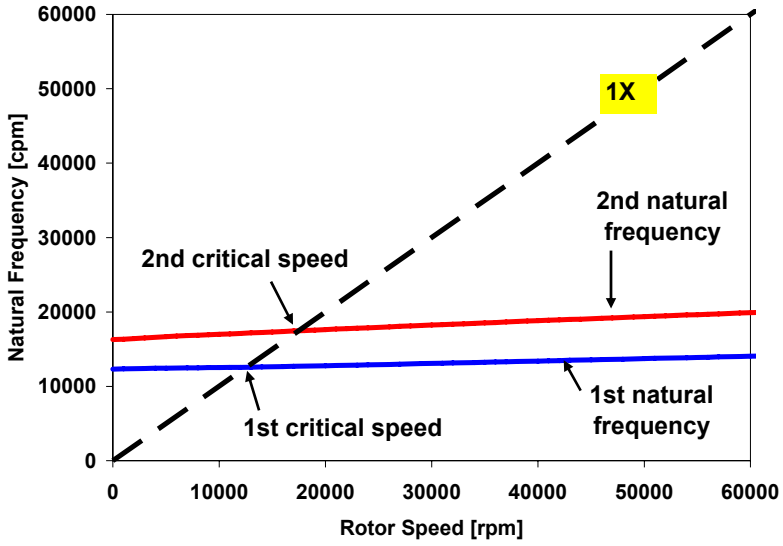

Fig. D.2 Predicted damped natural frequency map of test rotor-bearing system. 5.08 bar bearing feed pressure.

[24] The difference in bearing force coefficients between the left and right bearings renders two conical modes [9].

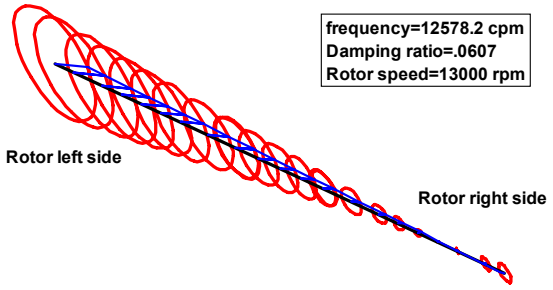

(a) First rigid body mode

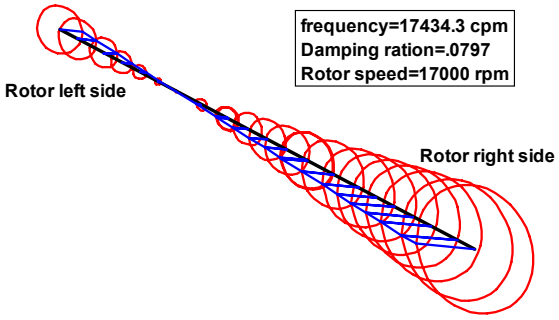

(b) Second rigid body mode

Fig. D.3 Mode shapes of test rotor at critical speeds. 5.08 bar bearing feed pressure.

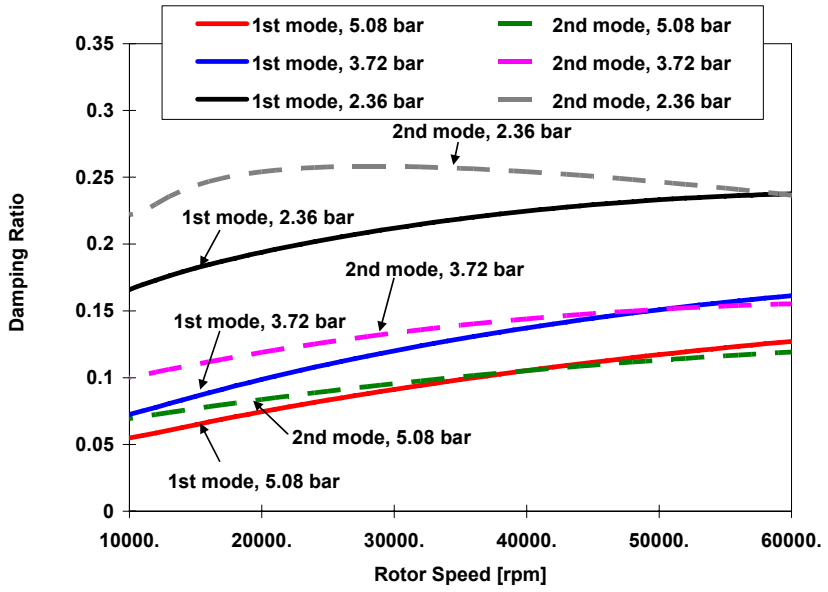

Fig. D.4 Predicted damping ratios of first and second rigid body mode versus rotor speed for three supply pressures into hybrid bearings.

Figure D.5 shows the predicted and measured synchronous rotor imbalance response for 2.36 bar and 5.08 bar (ab) feed pressure into the bearings. The rotor motion measurements are along the horizontal direction near the left and right bearings. From the recorded rotor responses, estimated imbalance masses are 0.05 gram·mm and 0.15 gram·mm at the left and right ends of the rotor respectively, and 55° in phase. The correlation of linear rotordynamic predictions to the measurements is remarkable.

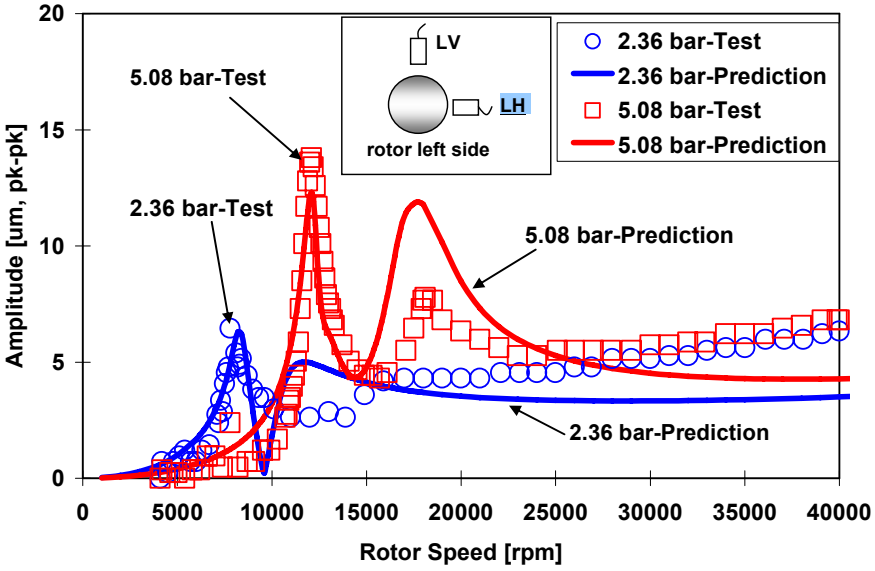

Fig. D. 5 Comparison of predicted and measured imbalance response of rotor. 2.36 bar and 5.08 bar bearing feed pressure. Left bearing horizontal direction (LH).